



Search for Gravitational Waves Associated with Gamma-Ray Bursts Detected by Fermi and Swift during the LIGO–Virgo Run O3a

R. Abbott¹, T. D. Abbott², S. Abraham³, F. Acernese^{4,5}, K. Ackley⁶ , C. Adams⁷, R. X. Adhikari¹, V. B. Adya⁸, C. Affeldt^{9,10}, M. Agathos^{11,12}, K. Agatsuma¹³ , N. Aggarwal¹⁴, O. D. Aguiar¹⁵, A. Aich¹⁶, L. Aiello^{17,18}, A. Ain³, P. Ajith¹⁹, G. Allen²⁰, A. Allocca²¹, P. A. Altin⁸, A. Amato²², S. Anand¹ , A. Ananyeva¹, S. B. Anderson¹, W. G. Anderson²³, S. V. Angelova²⁴, S. Ansoldi^{25,26}, S. Antier²⁷, S. Appert¹, K. Arai¹, M. C. Araya¹, J. S. Areeda²⁸, M. Arène²⁷, N. Arnaud^{29,30}, S. M. Aronson³¹, Y. Asali³², S. Ascenzi^{17,33}, G. Ashton⁶ , M. Assiduo^{5,34}, S. M. Aston⁷, P. Astone³⁵, F. Aubin³⁶ , P. Aufmuth¹⁰, K. AultO'Neal³⁷, C. Austin², V. Avendano³⁸, S. Babak²⁷, P. Bacon²⁷, F. Badaracco^{17,18} , M. K. M. Bader³⁹, S. Bae⁴⁰, A. M. Baer⁴¹, J. Baird²⁷, F. Baldaccini^{42,43}, G. Ballardin³⁰, S. W. Ballmer⁴⁴, A. Bals³⁷, A. Balsamo⁴¹, G. Baltus⁴⁵, S. Banagiri⁴⁶ , D. Bankar³, R. S. Bankar³, J. C. Barayoga¹, C. Barbieri^{47,48}, B. C. Barish¹, D. Barker⁴⁹, K. Barkett⁵⁰, P. Barneo⁵¹, F. Barone^{5,52}, B. Barr⁵³, L. Barsotti⁵⁴, M. Barsuglia²⁷, D. Barta⁵⁵, J. Bartlett⁴⁹, I. Bartos³¹ , R. Bassiri⁵⁶, A. Basti^{21,57}, M. Bawaj^{43,58}, J. C. Bayley⁵³, M. Bazzan^{59,60}, B. Bécsy⁶¹ , M. Bejger⁶² , I. Belahcene²⁹, A. S. Bell⁵³, D. Beniwal⁶³, M. G. Benjamin³⁷, J. D. Bentley¹³, F. Bergamin⁹, B. K. Berger⁵⁶, G. Bergmann^{9,10}, S. Bernuzzi¹¹ , C. P. L. Berry¹⁴, D. Bersanetti⁶⁴, A. Bertolini³⁹, J. Betzwieser⁷, R. Bhandare⁶⁵, A. V. Bhandari³, A. Bianchi^{5,34}, J. Bidler²⁸, E. Biggs²³, I. A. Bilenko⁶⁶ , G. Billingsley¹, R. Birney⁶⁷, O. Birnholtz^{68,69}, S. Biscans^{1,54}, M. Bischi^{70,71}, S. Biscoveanu⁵⁴, A. Bisht¹⁰, G. Bissenbayeva¹⁶, M. Bitossi^{21,30}, M. A. Bizouard⁷², J. K. Blackburn¹, J. Blackman⁵⁰, C. D. Blair⁷, D. G. Blair⁷³, R. M. Blair⁴⁹, F. Bobba^{74,75}, N. Bode^{9,10}, M. Boer⁷² , Y. Boetzel⁷⁶, G. Bogaert⁷², F. Bondu⁷⁷, E. Bonilla⁵⁶, R. Bonnand³⁶, P. Booker^{9,10}, B. A. Boom³⁹, R. Bork¹, V. Boschi²¹, S. Bose³, V. Bossilkov⁷³, J. Bosveld⁷³, Y. Bouffanais^{59,60} , A. Bozzi³⁰, C. Bradaschia²¹, P. R. Brady²³, A. Bramley⁷, M. Branchesi^{17,18}, J. E. Brau⁷⁸, M. Breschi¹¹, T. Briant⁷⁹, J. H. Briggs⁵³, F. Brighenti^{70,71} , A. Brillet⁷², M. Brinkmann^{9,10}, P. Brockill²³, A. F. Brooks¹, J. Brooks³⁰, D. D. Brown⁶³, S. Brunett¹, G. Bruno⁸⁰, R. Bruntz⁴¹, A. Buikema⁵⁴, T. Bulik⁸¹, H. J. Bulten^{39,82}, A. Buonanno^{83,84}, D. Buskulic³⁶, R. L. Byer⁵⁶, M. Cabero^{9,10} , L. Cadonati⁸⁵, G. Cagnoli⁸⁶, C. Cahillane¹, J. Calderón Bustillo⁶, J. D. Callaghan⁵³, T. A. Callister¹, E. Calloni^{5,34}, J. B. Camp⁸⁷, M. Canepa^{64,88}, G. Caneva Santoro^{35,89}, K. C. Cannon⁹⁰, H. Cao⁶³, J. Cao⁹¹, G. Carapella^{74,75}, F. Carbognani³⁰, S. Caride⁹², M. F. Carney¹⁴, G. Carullo^{21,57}, T. L. Carver⁹³, J. Casanueva Diaz²¹, C. Casentini^{33,94} , J. Castañeda⁵¹, S. Caudill³⁹, M. Cavaglia⁹⁵, F. Cavalier²⁹, R. Cavalieri³⁰, G. Cella²¹, P. Cerdá-Durán⁹⁶, E. Cesarini^{33,97}, O. Chaibi⁷², K. Chakravarti³, C. Chan⁹⁰, M. Chan⁵³, S. Chao⁹⁸, P. Charlton⁹⁹, E. A. Chase¹⁴ , E. Chassande-Mottin²⁷, D. Chatterjee²³, M. Chaturvedi⁶⁵, H. Y. Chen¹⁰⁰, X. Chen⁷³, Y. Chen⁵⁰, H.-P. Cheng³¹, C. K. Cheong¹⁰¹, H. Y. Chia³¹, F. Chiadini^{75,102}, R. Chierici¹⁰³, A. Chincarini⁶⁴, A. Chiummo³⁰, G. Cho¹⁰⁴, H. S. Cho¹⁰⁵, M. Cho⁸⁴, N. Christensen⁷², Q. Chu⁷³, S. Chua⁷⁹, K. W. Chung¹⁰¹, S. Chung⁷³, G. Ciani^{59,60}, P. Ciecielag⁶², M. Cieřlar⁶², A. A. Ciobanu⁶³, R. Ciolfi^{60,106}, F. Cipriano⁷², A. Cirone^{64,88}, F. Clara⁴⁹, J. A. Clark⁸⁵, P. Clearwater¹⁰⁷, S. Clesse⁸⁰, F. Cleva⁷², E. Coccia^{17,18}, P.-F. Cohadon⁷⁹, D. Cohen²⁹, M. Colleoni¹⁰⁸, C. G. Collette¹⁰⁹, C. Collins¹³, M. Colpi^{47,48}, M. Constance, Jr.¹⁵, L. Conti⁶⁰, S. J. Cooper¹³, P. Corban⁷, T. R. Corbitt², I. Cordero-Carrión¹¹⁰, S. Corezzi^{42,43}, K. R. Corley³², N. Cornish⁶¹, D. Corre²⁹, A. Corsi⁹² , S. Cortese³⁰, C. A. Costa¹⁵, R. Cotesta⁸³, M. W. Coughlin¹ , S. B. Coughlin^{14,93}, J.-P. Coulon⁷², S. T. Countryman³², P. Couvares¹, P. B. Covas¹⁰⁸, D. M. Coward⁷³, M. J. Cowart⁷, D. C. Coyne¹, R. Coyne¹¹¹, J. D. E. Creighton²³, T. D. Creighton¹⁶, J. Cripe², M. Croquette⁷⁹, S. G. Crowder¹¹², J.-R. Cudell⁴⁵, T. J. Cullen², A. Cumming⁵³ , R. Cummings⁵³, L. Cunningham⁵³, E. Cuoco³⁰, M. Curylo⁸¹, T. Dal Canton⁸³, G. Dálya¹¹³, A. Dana⁵⁶, L. M. Daneshgaran-Bajastani¹¹⁴, B. D'Angelo^{64,88}, S. L. Danilishin^{9,10}, S. D'Antonio³³, K. Danzmann^{9,10}, C. Darsow-Fromm¹¹⁵, A. Dasgupta¹¹⁶, L. E. H. Datrier⁵³, V. Dattilo³⁰, I. Dave⁶⁵, M. Davier²⁹, G. S. Davies¹¹⁷, D. Davis⁴⁴, E. J. Daw¹¹⁸, D. DeBra⁵⁶, M. Deenadayalan³, J. Degallaix²², M. De Laurentis^{5,34}, S. Deléglise⁷⁹, M. Delfavero⁶⁸, N. De Lillo⁵³, W. Del Pozzo^{21,57}, L. M. DeMarchi¹⁴, V. D'Emilio⁹³, N. Demos⁵⁴, T. Dent¹¹⁷, R. De Pietri^{119,120}, R. De Rosa^{5,34}, C. De Rossi³⁰, R. DeSalvo¹²¹, O. de Varona^{9,10}, S. Dhurandhar³, M. C. Díaz¹⁶, M. Diaz-Ortiz, Jr.³¹, T. Dietrich³⁹, L. Di Fiore⁵, C. Di Fronzo¹³, C. Di Giorgio^{74,75}, F. Di Giovanni⁹⁶, M. Di Giovanni^{122,123}, T. Di Girolamo^{5,34}, A. Di Lieto^{21,57}, B. Ding¹⁰⁹, S. Di Pace^{35,89}, I. Di Palma^{35,89}, F. Di Renzo^{21,57}, A. K. Divakarla³¹, A. Dmitriev¹³, Z. Doctor¹⁰⁰ , F. Donovan⁵⁴, K. L. Dooley⁹³, S. Doravari³, I. Dorrington⁹³, T. P. Downes²³, M. Drago^{17,18}, J. C. Driggers⁴⁹, Z. Du⁹¹, J.-G. Ducoin²⁹, P. Dupej⁵³, O. Durante^{74,75}, D. D'Urso^{124,125}, S. E. Dwyer⁴⁹, P. J. Easter⁶, G. Eddolls⁵³, B. Edelman⁷⁸, T. B. Edo¹¹⁸, O. Edy¹²⁶, A. Effler⁷, P. Ehrens¹, J. Eichholz⁸, S. S. Eikenberry³¹, M. Eisenmann³⁶, R. A. Eisenstein⁵⁴, A. Ejlli⁹³, L. Errico^{5,34}, R. C. Essick¹⁰⁰ , H. Estelles¹⁰⁸, D. Estevez³⁶, Z. B. Etienne¹²⁷, T. Etzel¹, M. Evans⁵⁴, T. M. Evans⁷ , B. E. Ewing¹²⁸, V. Fafone^{17,33,94}, S. Fairhurst⁹³, X. Fan⁹¹, S. Farinon⁶⁴, B. Farr⁷⁸ , W. M. Farr^{129,130} , E. J. Fauchon-Jones⁹³, M. Favata³⁸, M. Fays¹¹⁸, M. Fazio¹³¹, J. Feicht¹, M. M. Fejer⁵⁶, F. Feng²⁷ , E. Fenyvesi^{55,132}, D. L. Ferguson⁸⁵, A. Fernandez-Galiana⁵⁴, I. Ferrante^{21,57}, E. C. Ferreira¹⁵, T. A. Ferreira¹⁵, F. Fidecaro^{21,57}, I. Fiori³⁰, D. Fiorucci^{17,18}, M. Fishbach¹⁰⁰ , R. P. Fisher⁴¹, R. Fittipaldi^{75,133}, M. Fitz-Axen⁴⁶, V. Fiumara^{75,134}, R. Flaminio^{36,135}, E. Floden⁴⁶, E. Flynn²⁸, H. Fong⁹⁰, J. A. Font^{96,136}, P. W. F. Forsyth⁸, J.-D. Fournier⁷², S. Frasca^{35,89}, F. Frasconi²¹, Z. Frei¹¹³, A. Freise¹³, R. Frey⁷⁸, V. Frey²⁹, P. Fritschel⁵⁴, V. V. Frolov⁷, G. Fronzè¹³⁷, P. Fulda³¹, M. Fyffe⁷, H. A. Gabbard⁵³, B. U. Gadre⁸³, S. M. Gaebel¹³, J. R. Gair⁸³, S. Galadage⁶, D. Ganapathy⁵⁴, S. G. Gaonkar³, C. García-Quirós¹⁰⁸, F. Garufi^{5,34}, B. Gateley⁴⁹, S. Gaudio³⁷, V. Gayathri¹³⁸, G. Gemme⁶⁴, E. Genin³⁰, A. Gennai²¹, D. George²⁰, J. George⁶⁵, L. Gergely¹³⁹, S. Ghonge⁸⁵, Abhirup Ghosh⁸³, Archisman Ghosh^{39,140,141,142} , S. Ghosh²³, B. Giacomazzo^{122,123}, J. A. Giaime^{2,7}

K. D. Giardino⁷, D. R. Gibson⁶⁷, C. Gier²⁴, K. Gill³², J. Glanzer², J. Griesmer¹¹⁵, P. Godwin¹²⁸, E. Goetz^{2,95}, R. Goetz³¹, N. Gohlke^{9,10}, B. Goncharov⁶, G. González², A. Gopakumar¹⁴³, S. E. Gossan¹, M. Gosselin^{21,30,57}, R. Gouaty³⁶, B. Grace⁸, A. Grado^{5,144} , M. Granata²², A. Grant⁵³, S. Gras⁵⁴, P. Grassia¹, C. Gray⁴⁹, R. Gray⁵³, G. Greco^{70,71}, A. C. Green³¹, R. Green⁹³, E. M. Gretarsson³⁷, H. L. Griggs⁸⁵, G. Grignani^{42,43}, A. Grimaldi^{122,123}, S. J. Grimm^{17,18}, H. Grote⁹³, S. Grunewald⁸³, P. Gruning²⁹, G. M. Guidi^{70,71}, A. R. Guimaraes², G. Guixé⁵¹, H. K. Gulati¹¹⁶, Y. Guo³⁹, A. Gupta¹²⁸, Anchal Gupta¹, P. Gupta³⁹, E. K. Gustafson¹, R. Gustafson¹⁴⁵, L. Haegel¹⁰⁸, O. Halim^{17,18}, E. D. Hall⁵⁴, E. Z. Hamilton⁹³, G. Hammond⁵³, M. Haney⁷⁶, M. M. Hanke^{9,10}, J. Hanks⁴⁹, C. Hanna¹²⁸, M. D. Hannam⁹³, O. A. Hannuksela¹⁰¹, T. J. Hansen³⁷, J. Hanson⁷, T. Harder⁷², T. Hardwick², K. Haris¹⁹, J. Harms^{17,18}, G. M. Harry¹⁴⁶, I. W. Harry¹²⁶, R. K. Hasskew⁷, C.-J. Haster⁵⁴ , K. Haughian⁵³, F. J. Hayes⁵³, J. Healy⁶⁸, A. Heidmann⁷⁹, M. C. Heintze⁷, J. Heinze^{9,10}, H. Heitmann⁷², F. Hellman¹⁴⁷, P. Hello²⁹, G. Hemming³⁰, M. Hendry⁵³, I. S. Heng⁵³, E. Hennes³⁹, J. Hennig^{9,10}, M. Heurs^{9,10}, S. Hild^{53,148}, T. Hinderer^{39,140,142}, S. Y. Hoback^{28,146}, S. Hochheim^{9,10}, E. Hofgard⁵⁶, D. Hofman²², A. M. Holgado²⁰ , N. A. Holland⁸, K. Holt⁷, D. E. Holz¹⁰⁰ , P. Hopkins⁹³ , C. Horst²³, J. Hough⁵³, E. J. Howell⁷³, C. G. Hoy⁹³, Y. Huang⁵⁴, M. T. Hübner⁶, E. A. Huerta²⁰ , D. Huet²⁹, B. Hughey³⁷, V. Hui³⁶, S. Husa¹⁰⁸, S. H. Huttner⁵³, R. Huxford¹²⁸, T. Huynh-Dinh⁷, B. Idzkowski⁸¹, A. Iess^{33,94}, H. Inchauspe³¹, C. Ingram⁶³, G. Intini^{35,89}, J.-M. Isac⁷⁹, M. Isi⁵⁴, B. R. Iyer¹⁹, T. Jacqmin⁷⁹, S. J. Jadhav¹⁴⁹, S. P. Jadhav³, A. L. James⁹³, K. Jani⁸⁵, N. N. Janthaler¹⁴⁹, P. Jaranowski¹⁵⁰, D. Jariwala³¹, R. Jaume¹⁰⁸, A. C. Jenkins¹⁵¹, J. Jiang³¹, G. R. Johns⁴¹, A. W. Jones¹³, D. I. Jones¹⁵², J. D. Jones⁴⁹, P. Jones¹³, R. Jones⁵³, R. J. G. Jonker³⁹, L. Ju⁷³, J. Junker^{9,10}, C. V. Kalaghatgi⁹³, V. Kalogera¹⁴ , B. Kamai¹, S. Kandhasamy³, G. Kang⁴⁰, J. B. Kanner¹, S. J. Kapadia¹⁹ , S. Karki⁷⁸, R. Kashyap¹⁹, M. Kasprzak¹, W. Kastaun^{9,10}, S. Katsanevas³⁰, E. Katsavounidis⁵⁴, W. Katzman⁷, S. Kaufer¹⁰, K. Kawabe⁴⁹, F. Kéfélian⁷², D. Keitel¹²⁶, A. Keivani³² , R. Kennedy¹¹⁸, J. S. Key¹⁵³, S. Khadka⁵⁶, F. Y. Khalili⁶⁶, I. Khan^{17,33}, S. Khan^{9,10}, Z. A. Khan⁹¹, E. A. Khazanov¹⁵⁴, N. Khetan^{17,18}, M. Khursheed⁶⁵, N. Kijbunchoo⁸, Chunglee Kim¹⁵⁵, G. J. Kim⁸⁵, J. C. Kim¹⁵⁶, K. Kim¹⁰¹, W. Kim⁶³, W. S. Kim¹⁵⁷, Y.-M. Kim¹⁵⁸, C. Kimball¹⁴, P. J. King⁴⁹, M. Kinley-Hanlon⁵³, R. Kirchhoff^{9,10}, J. S. Kissel⁴⁹, L. Kleybolte¹¹⁵, S. Klimenko³¹, T. D. Knowles¹²⁷, E. Knyazev⁵⁴, P. Koch^{9,10} , S. M. Koehlenbeck^{9,10}, G. Koekoek^{39,148}, S. Koley³⁹, V. Kondrashov¹, A. Kontos¹⁵⁹, N. Koper^{9,10}, M. Korobko¹¹⁵, W. Z. Korth¹, M. Kovalam⁷³, D. B. Kozak¹, V. Kringel^{9,10}, N. V. Krishnendu¹⁶⁰, A. Królak^{161,162}, N. Krupinski²³, G. Kuehn^{9,10}, A. Kumar¹⁴⁹, P. Kumar¹⁶³, Rahul Kumar⁴⁹, Rakesh Kumar¹¹⁶, S. Kumar¹⁹, L. Kuo⁹⁸, A. Kutynia¹⁶¹, B. D. Lackey⁸³, D. Laghi^{21,57}, E. Lalande¹⁶⁴, T. L. Lam¹⁰¹, A. Lamberts^{72,165}, M. Landry⁴⁹, B. B. Lane⁵⁴, R. N. Lang¹⁶⁶, J. Lange⁶⁸, B. Lantz⁵⁶, R. K. Lanza⁵⁴, I. La Rosa³⁶, A. Lartaux-Vollard²⁹, P. D. Lasky⁶, M. Laxen⁷, A. Lazzarini¹, C. Lazzaro⁶⁰, P. Leaci^{35,89}, S. Leavey^{9,10}, Y. K. Lecoecuche⁴⁹, C. H. Lee¹⁰⁵, H. M. Lee¹⁶⁷, H. W. Lee¹⁵⁶, J. Lee¹⁰⁴, K. Lee⁵⁶, J. Lehmann^{9,10}, N. Leroy²⁹, N. Letendre³⁶, Y. Levin⁶, A. K. Y. Li¹⁰¹, J. Li⁹¹, K. li¹⁰¹, T. G. F. Li¹⁰¹, X. Li⁵⁰, F. Linde^{39,168}, S. D. Linker¹¹⁴, J. N. Linley⁵³, T. B. Littenberg¹⁶⁹, J. Liu^{9,10}, X. Liu²³, M. Llorens-Monteaudo⁹⁶, R. K. L. Lo¹, A. Lockwood¹⁷⁰, L. T. London⁵⁴, A. Longo^{171,172}, M. Lorenzini^{17,18}, V. Lorette¹⁷³, M. Lormand⁷, G. Losurdo²¹, J. D. Lough^{9,10}, C. O. Lousto⁶⁸ , G. Lovelace²⁸, H. Lück^{9,10}, D. Lumaca^{33,94}, A. P. Lundgren¹²⁶, Y. Ma⁵⁰, R. Macas⁹³, S. Macfoy²⁴, M. MacInnis⁵⁴, D. M. Macleod⁹³, I. A. O. MacMillan¹⁴⁶, A. Macquet⁷², I. Magaña Hernandez²³, F. Magaña-Sandoval³¹, R. M. Magee¹²⁸ , E. Majorana³⁵, I. Maksimovic¹⁷³, A. Malik⁶⁵, N. Man⁷², V. Mandic⁴⁶, V. Mangano^{35,53,89}, G. L. Mansell^{49,54}, M. Manske²³, M. Mantovani³⁰, M. Mapelli^{59,60}, F. Marchesoni^{43,58,174}, F. Marion³⁶, S. Márka³², Z. Márka³², C. Markakis¹², A. S. Markosyan⁵⁶, A. Markowitz¹ , E. Maros¹, A. Marquina¹¹⁰, S. Marsat²⁷, F. Martelli^{70,71}, I. W. Martin⁵³, R. M. Martin³⁸, V. Martinez⁸⁶, D. V. Martynov¹³, H. Masalehdan¹¹⁵, K. Mason⁵⁴, E. Massera¹¹⁸, A. Masserot³⁶, T. J. Massinger⁵⁴, M. Masso-Reid⁵³, S. Mastrogiovanni²⁷, A. Matas⁸³, F. Matichard^{1,54}, N. Mavalvala⁵⁴, E. Maynard², J. J. McCann⁷³, R. McCarthy⁴⁹, D. E. McClelland⁸, S. McCormick⁷, L. McCuller⁵⁴, S. C. McGuire¹⁷⁵, C. McIsaac¹²⁶, J. McIver¹, D. J. McManus⁸, T. McRae⁸, S. T. McWilliams¹²⁷, D. Meacher²³, G. D. Meadors⁶, M. Mehmet^{9,10}, A. K. Mehta¹⁹, E. Mejuto Villa^{75,121}, A. Melatos¹⁰⁷, G. Mendell⁴⁹, R. A. Mercer²³, L. Mereni²², K. Merfeld⁷⁸, E. L. Merilh⁴⁹, J. D. Merritt⁷⁸, M. Merzougui⁷², S. Meshkov¹, C. Messenger⁵³, C. Messick¹⁷⁶, R. Metzдорff⁷⁹, P. M. Meyers¹⁰⁷, F. Meylahn^{9,10}, A. Mhaske³, A. Miani^{122,123}, H. Miao¹³, I. Michaloliakos³¹, C. Michel²², H. Middleton¹⁰⁷, L. Milano^{5,34}, A. L. Miller^{31,35,89}, M. Millhouse¹⁰⁷, J. C. Mills⁹³, E. Milotti^{26,177}, M. C. Milovich-Goff¹¹⁴, O. Minazzoli^{72,178}, Y. Minenkov³³, A. Mishkin³¹, C. Mishra¹⁷⁹, T. Mistry¹¹⁸, S. Mitra³, V. P. Mitrofanov⁶⁶, G. Mitselmakher³¹, R. Mittleman⁵⁴, G. Mo⁵⁴, K. Mogushi⁹⁵, S. R. P. Mohapatra⁵⁴, S. R. Mohite²³, M. Molina-Ruiz¹⁴⁷, M. Mondin¹¹⁴, M. Montani^{70,71}, C. J. Moore¹³, D. Moraru⁴⁹, F. Morawski⁶², G. Moreno⁴⁹, S. Morisaki⁹⁰, B. Mours¹⁸⁰, C. M. Mow-Lowry¹³, S. Mozzon¹²⁶, F. Muciaccia^{35,89}, Arunava Mukherjee⁵³, D. Mukherjee¹²⁸, S. Mukherjee¹⁶, Subroto Mukherjee¹¹⁶, N. Mukund^{9,10}, A. Mullavey⁷, J. Munch⁶³, E. A. Muñoz⁴⁴, P. G. Murray⁵³, A. Nagar^{97,137,181}, I. Nardecchia^{33,94}, L. Naticchioni^{35,89}, R. K. Nayak¹⁸², B. F. Neil⁷³, J. Neilson^{75,121}, G. Nelemans^{39,183}, T. J. N. Nelson⁷, M. Nery^{9,10}, A. Neunert¹⁴⁵, K. Y. Ng⁵⁴, S. Ng⁶³, C. Nguyen²⁷, P. Nguyen⁷⁸, D. Nichols^{39,142}, S. A. Nichols², S. Nissanke^{39,142} , F. Nocera³⁰, M. Noh⁵⁴, C. North⁹³, D. Nothard¹⁸⁴, L. K. Nuttall¹²⁶, J. Oberling⁴⁹, B. D. O'Brien³¹, G. Oganessian^{17,18} , G. H. Ogin¹⁸⁵, J. J. Oh¹⁵⁷, S. H. Oh¹⁵⁷, F. Ohme^{9,10}, H. Ohta⁹⁰, M. A. Okada¹⁵, M. Oliver¹⁰⁸, C. Olivetto³⁰, P. Oppermann^{9,10}, Richard J. Oram⁷, B. O'Reilly⁷, R. G. Ormiston⁴⁶, N. Ormsby⁴¹, L. F. Ortega³¹, R. O'Shaughnessy⁶⁸ , S. Ossokine⁸³, C. Osthelder¹, D. J. Ottaway⁶³, H. Overmier⁷, B. J. Owen⁹², A. E. Pace¹²⁸, G. Pagano^{21,57}, M. A. Page⁷³, G. Pagliaroli^{17,18}, A. Pai¹³⁸, S. A. Pai⁶⁵, J. R. Palamos⁷⁸, O. Palashov¹⁵⁴, C. Palomba³⁵, H. Pan⁹⁸, P. K. Panda¹⁴⁹, P. T. H. Pang³⁹, C. Pankow¹⁴, F. Pannarale^{35,89}, B. C. Pant⁶⁵, F. Paoletti²¹, A. Paoli³⁰, A. Parida³, W. Parker^{7,175}, D. Pascucci^{39,53}, A. Pasqualetti³⁰, R. Passaquieti^{21,57}, D. Passuello²¹, M. Patel⁴¹, B. Patricelli^{21,57}, E. Payne⁶, B. L. Pearlstone⁵³, T. C. Pechsiri³¹, A. J. Pedersen⁴⁴, M. Pedraza¹, A. Pele⁷, S. Penn¹⁸⁶, A. Perego^{122,123}, C. J. Perez⁴⁹, C. Périgois³⁶, A. Perreca^{122,123}, S. Perriès¹⁰³, J. Petermann¹¹⁵

H. P. Pfeiffer⁸³, M. Phelps^{9,10}, K. S. Phukon^{3,39,168}, O. J. Piccinni^{35,89}, M. Pichot⁷², M. Piendibene^{21,57}, F. Piergiovanni^{70,71}, V. Piero^{75,121}, G. Pillant³⁰, L. Pinard²², I. M. Pinto^{75,97,121}, K. Piotrkowski⁸⁰, M. Pirello⁴⁹, M. Pitkin¹⁸⁷, W. Plastino^{171,172}, R. Poggiani^{21,57}, D. Y. T. Pong¹⁰¹, S. Ponrathnam³, P. Popolizio³⁰, E. K. Porter²⁷, J. Powell¹⁸⁸, A. K. Prajapati¹¹⁶, K. Prasai⁵⁶, R. Prasanna¹⁴⁹, G. Pratten¹³, T. Prestegard²³, M. Principe^{75,97,121}, G. A. Prodi^{122,123}, L. Prokhorov¹³, M. Punturo⁴³, P. Puppo³⁵, M. Pürer⁸³, H. Qi⁹³, V. Quetschke¹⁶, P. J. Quinonez³⁷, F. J. Raab⁴⁹, G. Raaijmakers^{39,142}, H. Radkins⁴⁹, N. Radulesco⁷², P. Raffai¹¹³, H. Rafferty¹⁸⁹, S. Raja⁶⁵, C. Rajan⁶⁵, B. Rajbhandari⁹², M. Rakhmanov¹⁶, K. E. Ramirez¹⁶, A. Ramos-Buades¹⁰⁸, Javed Rana³, K. Rao¹⁴, P. Rapagnani^{35,89}, V. Raymond⁹³, M. Razzano^{21,57}, J. Read²⁸, T. Regimbau³⁶, L. Rei⁶⁴, S. Reid²⁴, D. H. Reitze^{1,31}, P. Retegno^{137,190}, F. Ricci^{35,89}, C. J. Richardson³⁷, J. W. Richardson¹, P. M. Ricker²⁰, G. Riemenschneider^{137,190}, K. Riles¹⁴⁵, M. Rizzo¹⁴, N. A. Robertson^{1,53}, F. Robinet²⁹, A. Rocchi³³, R. D. Rodriguez-Soto³⁷, L. Rolland³⁶, J. G. Rollins¹, V. J. Roma⁷⁸, M. Romanelli⁷⁷, R. Romano^{4,5}, C. L. Romel⁴⁹, I. M. Romero-Shaw⁶, J. H. Romie⁷, C. A. Rose²³, D. Rose²⁸, K. Rose¹⁸⁴, D. Rosińska⁸¹, S. G. Rosofsky²⁰, M. P. Ross¹⁷⁰, S. Rowan⁵³, S. J. Rowlinson¹³, P. K. Roy¹⁶, Santosh Roy³, Soumen Roy¹⁹¹, P. Ruggi³⁰, G. Rutins⁶⁷, K. Ryan⁴⁹, S. Sachdev¹²⁸, T. Sadecki⁴⁹, M. Sakellariadou¹⁵¹, O. S. Salafia^{47,48,192}, L. Salconi³⁰, M. Saleem¹⁶⁰, A. Samajdar³⁹, E. J. Sanchez¹, L. E. Sanchez¹, N. Sanchis-Gual¹⁹³, J. R. Sanders¹⁹⁴, K. A. Santiago³⁸, E. Santos⁷², N. Sarin⁶, B. Sassolas²², B. S. Sathyaprakash^{93,128}, O. Sauter³⁶, R. L. Savage⁴⁹, V. Savant³, D. Sawant¹³⁸, S. Sayah²², D. Schaetzl¹, P. Schale⁷⁸, M. Scheel⁵⁰, J. Scheuer¹⁴, P. Schmidt¹³, R. Schnabel¹¹⁵, R. M. S. Schofield⁷⁸, A. Schönbeck¹¹⁵, E. Schreiber^{9,10}, B. W. Schulte^{9,10}, B. F. Schutz⁹³, O. Schwarm¹⁸⁵, E. Schwartz⁷, J. Scott⁵³, S. M. Scott⁸, E. Seidel²⁰, D. Sellers⁷, A. S. Sengupta¹⁹¹, N. Sennett⁸³, D. Sentenac³⁰, V. Sequino⁶⁴, A. Sergeev¹⁵⁴, Y. Setyawati^{9,10}, D. A. Shaddock⁸, T. Shaffer⁴⁹, M. S. Shahriar¹⁴, S. Sharif², A. Sharma^{17,18}, P. Sharma⁶⁵, P. Shawhan⁸⁴, H. Shen²⁰, M. Shikauchi⁹⁰, R. Shink¹⁶⁴, D. H. Shoemaker⁵⁴, D. M. Shoemaker⁸⁵, K. Shukla¹⁴⁷, S. ShyamSundar⁶⁵, K. Siellez⁸⁵, M. Sieniawska⁶², D. Sigg⁴⁹, L. P. Singer⁸⁷, D. Singh¹²⁸, N. Singh⁸¹, A. Singha⁵³, A. Singhal^{17,35}, A. M. Sintès¹⁰⁸, V. Sipala^{124,125}, V. Skliris⁹³, B. J. J. Slagmolen⁸, T. J. Slaven-Blair⁷³, J. Smetana¹³, J. R. Smith²⁸, R. J. E. Smith⁶, S. Somala¹⁹⁵, E. J. Son¹⁵⁷, S. Soni², B. Sorazu⁵³, V. Sordini¹⁰³, F. Sorrentino⁶⁴, T. Souradeep³, E. Sowell⁹², A. P. Spencer⁵³, M. Spera^{59,60}, A. K. Srivastava¹¹⁶, V. Srivastava⁴⁴, K. Staats¹⁴, C. Stachie⁷², M. Standke^{9,10}, D. A. Steer²⁷, M. Steinke^{9,10}, J. Steinlechner^{53,115}, S. Steinlechner¹¹⁵, D. Steinmeyer^{9,10}, D. Stocks⁵⁶, D. J. Stops¹³, M. Stover¹⁸⁴, K. A. Strain⁵³, G. Stratta^{71,196}, A. Strunk⁴⁹, R. Sturani¹⁹⁷, A. L. Stuver¹⁹⁸, S. Sudhagar³, V. Sudhir⁵⁴, T. Z. Summerscales¹⁹⁹, L. Sun¹, S. Sunil¹¹⁶, A. Sur⁶², J. Suresh⁹⁰, P. J. Sutton⁹³, B. L. Swinkels³⁹, M. J. Szczepańczyk³¹, M. Tacca³⁹, S. C. Tait⁵³, C. Talbot⁶, A. J. Tanasijczuk⁸⁰, D. B. Tanner³¹, D. Tao¹, M. Tápai¹³⁹, A. Tapia²⁸, E. N. Tapia San Martín³⁹, J. D. Tasson²⁰⁰, R. Taylor¹, R. Tenorio¹⁰⁸, L. Terkowski¹¹⁵, M. P. Thiruganasambandam³, M. Thomas⁷, P. Thomas⁴⁹, J. E. Thompson⁹³, S. R. Thondapu⁶⁵, K. A. Thorne⁷, E. Thrane⁶, C. L. Tinsman⁶, T. R. Saravanan³, Shubhanshu Tiwari^{76,122,123}, S. Tiwari¹⁴³, V. Tiwari⁹³, K. Toland⁵³, M. Tonelli^{21,57}, Z. Tornasi⁵³, A. Torres-Forné⁸³, C. I. Torrie¹, I. Tosta e Melo^{124,125}, D. Töyrä⁸, F. Travasso^{43,58}, G. Traylor⁷, M. C. Tringali⁸¹, A. Tripathi¹⁴⁵, A. Trovato²⁷, R. J. Trudeau¹, K. W. Tsang³⁹, M. Tse⁵⁴, R. Tso⁵⁰, L. Tsukada⁹⁰, D. Tsuna⁹⁰, T. Tsutsui⁹⁰, M. Turconi⁷², A. S. Ubhi¹³, K. Ueno⁹⁰, D. Ugolini¹⁸⁹, C. S. Unnikrishnan¹⁴³, A. L. Urban², S. A. Usman¹⁰⁰, A. C. Utina⁵³, H. Vahlbruch¹⁰, G. Vajente¹, G. Valdes², M. Valentini^{122,123}, N. van Bakel³⁹, M. van Beuzekom³⁹, J. F. J. van den Brand^{39,82,148}, C. Van Den Broeck^{39,201}, D. C. Vander-Hyde⁴⁴, L. van der Schaaf³⁹, J. V. Van Heijningen⁷³, A. A. van Veggel⁵³, M. Vardaro^{39,168}, V. Varma⁵⁰, S. Vass¹, M. Vasúth⁵⁵, A. Vecchio¹³, G. Vedovato⁶⁰, J. Veitch⁵³, P. J. Veitch⁶³, K. Venkateswara¹⁷⁰, G. Venugopalan¹, D. Verkindt³⁶, D. Veske³², F. Vetranò^{70,71}, A. Vicere^{70,71}, A. D. Viets²⁰², S. Vinciguerra¹³, D. J. Vine⁶⁷, J.-Y. Vinet⁷², S. Vitale⁵⁴, Francisco Hernandez Vivanco⁶, T. Vo⁴⁴, H. Vocca^{42,43}, C. Vorvick⁴⁹, S. P. Vyatchanin⁶⁶, A. R. Wade⁸, L. E. Wade¹⁸⁴, M. Wade¹⁸⁴, R. Walet³⁹, M. Walker²⁸, G. S. Wallace²⁴, L. Wallace¹, S. Walsh²³, J. Z. Wang¹⁴⁵, S. Wang²⁰, W. H. Wang¹⁶, R. L. Ward⁸, Z. A. Warden³⁷, J. Warner⁴⁹, M. Was³⁶, J. Watchi¹⁰⁹, B. Weaver⁴⁹, L.-W. Wei^{9,10}, M. Weinert^{9,10}, A. J. Weinstein¹, R. Weiss⁵⁴, F. Wellmann^{9,10}, L. Wen⁷³, P. Weßels^{9,10}, J. W. Westhouse³⁷, K. Wette⁸, J. T. Whelan⁶⁸, B. F. Whiting³¹, C. Whittle⁵⁴, D. M. Wilken^{9,10}, D. Williams⁵³, A. R. Williamson^{39,142}, J. L. Willis¹, B. Willke^{9,10}, W. Winkler^{9,10}, C. C. Wipf¹, H. Wittel^{9,10}, G. Woan⁵³, J. Woehler^{9,10}, J. K. Wofford⁶⁸, I. C. F. Wong¹⁰¹, J. L. Wright⁵³, D. S. Wu^{9,10}, D. M. Wysocki⁶⁸, L. Xiao¹, H. Yamamoto¹, L. Yang¹³¹, Y. Yang³¹, Z. Yang⁴⁶, M. J. Yap⁸, M. Yazback³¹, D. W. Yeeles⁹³, Hang Yu⁵⁴, Haocun Yu⁵⁴, S. H. R. Yuen¹⁰¹, A. K. Zadrożny¹⁶, A. Zadrożny¹⁶¹, M. Zanolin³⁷, T. Zelenova³⁰, J.-P. Zendri⁶⁰, M. Zevin¹⁴, J. Zhang⁷³, L. Zhang¹, T. Zhang⁵³, C. Zhao⁷³, G. Zhao¹⁰⁹, Y. Zheng⁹⁵, M. Zhou¹⁴, Z. Zhou¹⁴, X. J. Zhu⁶, M. E. Zucker^{1,54}, and J. Zweigig¹

The LIGO Scientific Collaboration and the Virgo Collaboration²⁰³

¹ LIGO, California Institute of Technology, Pasadena, CA 91125, USA

² Louisiana State University, Baton Rouge, LA 70803, USA

³ Inter-University Centre for Astronomy and Astrophysics, Pune 411007, India

⁴ Dipartimento di Farmacia, Università di Salerno, I-84084 Fisciano, Salerno, Italy

⁵ INFN, Sezione di Napoli, Complesso Universitario di Monte S. Angelo, I-80126 Napoli, Italy

⁶ OzGrav, School of Physics & Astronomy, Monash University, Clayton 3800, Victoria, Australia

⁷ LIGO Livingston Observatory, Livingston, LA 70754, USA

⁸ OzGrav, Australian National University, Canberra, Australian Capital Territory 0200, Australia

⁹ Max Planck Institute for Gravitational Physics (Albert Einstein Institute), D-30167 Hannover, Germany

¹⁰ Leibniz Universität Hannover, D-30167 Hannover, Germany

¹¹ Theoretisch-Physikalisches Institut, Friedrich-Schiller-Universität Jena, D-07743 Jena, Germany

¹² University of Cambridge, Cambridge CB2 1TN, UK

¹³ University of Birmingham, Birmingham B15 2TT, UK

¹⁴ Center for Interdisciplinary Exploration & Research in Astrophysics (CIERA), Northwestern University, Evanston, IL 60208, USA

¹⁵ Instituto Nacional de Pesquisas Espaciais, 12227-010 São José dos Campos, São Paulo, Brazil

- ¹⁶ The University of Texas Rio Grande Valley, Brownsville, TX 78520, USA
¹⁷ Gran Sasso Science Institute (GSSI), I-67100 L'Aquila, Italy
¹⁸ INFN, Laboratori Nazionali del Gran Sasso, I-67100 Assergi, Italy
¹⁹ International Centre for Theoretical Sciences, Tata Institute of Fundamental Research, Bengaluru 560089, India
²⁰ NCSA, University of Illinois at Urbana-Champaign, Urbana, IL 61801, USA
²¹ INFN, Sezione di Pisa, I-56127 Pisa, Italy
²² Laboratoire des Matériaux Avancés (LMA), IP2I—UMR 5822, CNRS, Université de Lyon, F-69622 Villeurbanne, France
²³ University of Wisconsin-Milwaukee, Milwaukee, WI 53201, USA
²⁴ SUPA, University of Strathclyde, Glasgow G1 1XQ, UK
²⁵ Dipartimento di Matematica e Informatica, Università di Udine, I-33100 Udine, Italy
²⁶ INFN, Sezione di Trieste, I-34127 Trieste, Italy
²⁷ APC, AstroParticule et Cosmologie, Université Paris Diderot, CNRS/IN2P3, CEA/Irfu, Observatoire de Paris, Sorbonne Paris Cité, F-75205 Paris Cedex 13, France
²⁸ California State University Fullerton, Fullerton, CA 92831, USA
²⁹ LAL, Univ. Paris-Sud, CNRS/IN2P3, Université Paris-Saclay, F-91898 Orsay, France
³⁰ European Gravitational Observatory (EGO), I-56021 Cascina, Pisa, Italy
³¹ University of Florida, Gainesville, FL 32611, USA
³² Columbia University, New York, NY 10027, USA
³³ INFN, Sezione di Roma Tor Vergata, I-00133 Roma, Italy
³⁴ Università di Napoli “Federico II,” Complesso Universitario di Monte S. Angelo, I-80126 Napoli, Italy
³⁵ INFN, Sezione di Roma, I-00185 Roma, Italy
³⁶ Laboratoire d’Annecy de Physique des Particules (LAPP), Univ. Grenoble Alpes, Université Savoie Mont Blanc, CNRS/IN2P3, F-74941 Annecy, France
³⁷ Embry-Riddle Aeronautical University, Prescott, AZ 86301, USA
³⁸ Montclair State University, Montclair, NJ 07043, USA
³⁹ Nikhef, Science Park 105, 1098 XG Amsterdam, The Netherlands
⁴⁰ Korea Institute of Science and Technology Information, Daejeon 34141, Republic of Korea
⁴¹ Christopher Newport University, Newport News, VA 23606, USA
⁴² Università di Perugia, I-06123 Perugia, Italy
⁴³ INFN, Sezione di Perugia, I-06123 Perugia, Italy
⁴⁴ Syracuse University, Syracuse, NY 13244, USA
⁴⁵ Université de Liège, B-4000 Liège, Belgium
⁴⁶ University of Minnesota, Minneapolis, MN 55455, USA
⁴⁷ Università degli Studi di Milano-Bicocca, I-20126 Milano, Italy
⁴⁸ INFN, Sezione di Milano-Bicocca, I-20126 Milano, Italy
⁴⁹ LIGO Hanford Observatory, Richland, WA 99352, USA
⁵⁰ Caltech CaRT, Pasadena, CA 91125, USA
⁵¹ Departament de Física Quàntica i Astrofísica, Institut de Ciències del Cosmos (ICCUB), Universitat de Barcelona (IEEC-UB), E-08028 Barcelona, Spain
⁵² Dipartimento di Medicina, Chirurgia e Odontoiatria “Scuola Medica Salernitana,” Università di Salerno, I-84081 Baronissi, Salerno, Italy
⁵³ SUPA, University of Glasgow, Glasgow G12 8QQ, UK
⁵⁴ LIGO, Massachusetts Institute of Technology, Cambridge, MA 02139, USA
⁵⁵ Wigner RCP, RMKI, H-1121 Budapest, Konkoly Thege Miklós út 29-33, Hungary
⁵⁶ Stanford University, Stanford, CA 94305, USA
⁵⁷ Università di Pisa, I-56127 Pisa, Italy
⁵⁸ Università di Camerino, Dipartimento di Fisica, I-62032 Camerino, Italy
⁵⁹ Università di Padova, Dipartimento di Fisica e Astronomia, I-35131 Padova, Italy
⁶⁰ INFN, Sezione di Padova, I-35131 Padova, Italy
⁶¹ Montana State University, Bozeman, MT 59717, USA
⁶² Nicolaus Copernicus Astronomical Center, Polish Academy of Sciences, 00-716, Warsaw, Poland
⁶³ OzGrav, University of Adelaide, Adelaide, South Australia 5005, Australia
⁶⁴ INFN, Sezione di Genova, I-16146 Genova, Italy
⁶⁵ RRCAT, Indore, Madhya Pradesh 452013, India
⁶⁶ Faculty of Physics, Lomonosov Moscow State University, Moscow 119991, Russia
⁶⁷ SUPA, University of the West of Scotland, Paisley PA1 2BE, UK
⁶⁸ Rochester Institute of Technology, Rochester, NY 14623, USA
⁶⁹ Bar-Ilan University, Ramat Gan 5290002, Israel
⁷⁰ Università degli Studi di Urbino “Carlo Bo,” I-61029 Urbino, Italy
⁷¹ INFN, Sezione di Firenze, I-50019 Sesto Fiorentino, Firenze, Italy
⁷² Artemis, Université Côte d’Azur, Observatoire Côte d’Azur, CNRS, CS 34229, F-06304 Nice Cedex 4, France
⁷³ OzGrav, University of Western Australia, Crawley, Western Australia 6009, Australia
⁷⁴ Dipartimento di Fisica “E.R. Caianiello,” Università di Salerno, I-84084 Fisciano, Salerno, Italy
⁷⁵ INFN, Sezione di Napoli, Gruppo Collegato di Salerno, Complesso Universitario di Monte S. Angelo, I-80126 Napoli, Italy
⁷⁶ Physik-Institut, University of Zurich, Winterthurerstrasse 190, 8057 Zurich, Switzerland
⁷⁷ Univ Rennes, CNRS, Institut FOTON—UMR6082, F-3500 Rennes, France
⁷⁸ University of Oregon, Eugene, OR 97403, USA
⁷⁹ Laboratoire Kastler Brossel, Sorbonne Université, CNRS, ENS-Université PSL, Collège de France, F-75005 Paris, France
⁸⁰ Université catholique de Louvain, B-1348 Louvain-la-Neuve, Belgium
⁸¹ Astronomical Observatory Warsaw University, 00-478 Warsaw, Poland
⁸² VU University Amsterdam, 1081 HV Amsterdam, The Netherlands
⁸³ Max Planck Institute for Gravitational Physics (Albert Einstein Institute), D-14476 Potsdam-Golm, Germany
⁸⁴ University of Maryland, College Park, MD 20742, USA
⁸⁵ School of Physics, Georgia Institute of Technology, Atlanta, GA 30332, USA
⁸⁶ Université de Lyon, Université Claude Bernard Lyon 1, CNRS, Institut Lumière Matière, F-69622 Villeurbanne, France
⁸⁷ NASA Goddard Space Flight Center, Greenbelt, MD 20771, USA
⁸⁸ Dipartimento di Fisica, Università degli Studi di Genova, I-16146 Genova, Italy
⁸⁹ Università di Roma “La Sapienza,” I-00185 Roma, Italy
⁹⁰ RESCEU, University of Tokyo, Tokyo, 113-0033, Japan

- ⁹¹ Tsinghua University, Beijing 100084, People's Republic of China
- ⁹² Texas Tech University, Lubbock, TX 79409, USA
- ⁹³ Cardiff University, Cardiff CF24 3AA, UK
- ⁹⁴ Università di Roma Tor Vergata, I-00133 Roma, Italy
- ⁹⁵ Missouri University of Science and Technology, Rolla, MO 65409, USA
- ⁹⁶ Departamento de Astronomía y Astrofísica, Universitat de València, E-46100 Burjassot, València, Spain
- ⁹⁷ Museo Storico della Fisica e Centro Studi e Ricerche "Enrico Fermi," I-00184 Roma, Italy
- ⁹⁸ National Tsing Hua University, Hsinchu City, 30013 Taiwan, People's Republic of China
- ⁹⁹ Charles Sturt University, Wagga Wagga, New South Wales 2678, Australia
- ¹⁰⁰ University of Chicago, Chicago, IL 60637, USA
- ¹⁰¹ The Chinese University of Hong Kong, Shatin, NT, Hong Kong
- ¹⁰² Dipartimento di Ingegneria Industriale (DIIN), Università di Salerno, I-84084 Fisciano, Salerno, Italy
- ¹⁰³ Institut de Physique des 2 Infinis de Lyon (IP2I) - UMR 5822, Université de Lyon, Université Claude Bernard, CNRS, F-69622 Villeurbanne, France
- ¹⁰⁴ Seoul National University, Seoul 08826, Republic of Korea
- ¹⁰⁵ Pusan National University, Busan 46241, Republic of Korea
- ¹⁰⁶ INAF, Osservatorio Astronomico di Padova, I-35122 Padova, Italy
- ¹⁰⁷ OzGrav, University of Melbourne, Parkville, Victoria 3010, Australia
- ¹⁰⁸ Universitat de les Illes Balears, IAC3—IEEC, E-07122 Palma de Mallorca, Spain
- ¹⁰⁹ Université Libre de Bruxelles, Brussels B-1050, Belgium
- ¹¹⁰ Departamento de Matemáticas, Universitat de València, E-46100 Burjassot, València, Spain
- ¹¹¹ University of Rhode Island, Kingston, RI 02881, USA
- ¹¹² Bellevue College, Bellevue, WA 98007, USA
- ¹¹³ MTA-ELTE Astrophysics Research Group, Institute of Physics, Eötvös University, Budapest 1117, Hungary
- ¹¹⁴ California State University, Los Angeles, 5151 State University Dr, Los Angeles, CA 90032, USA
- ¹¹⁵ Universität Hamburg, D-22761 Hamburg, Germany
- ¹¹⁶ Institute for Plasma Research, Bhat, Gandhinagar 382428, India
- ¹¹⁷ IGFAE, Campus Sur, Universidade de Santiago de Compostela, E-15782, Spain
- ¹¹⁸ The University of Sheffield, Sheffield S10 2TN, UK
- ¹¹⁹ Dipartimento di Scienze Matematiche, Fisiche e Informatiche, Università di Parma, I-43124 Parma, Italy
- ¹²⁰ INFN, Sezione di Milano Bicocca, Gruppo Collegato di Parma, I-43124 Parma, Italy
- ¹²¹ Dipartimento di Ingegneria, Università del Sannio, I-82100 Benevento, Italy
- ¹²² Università di Trento, Dipartimento di Fisica, I-38123 Povo, Trento, Italy
- ¹²³ INFN, Trento Institute for Fundamental Physics and Applications, I-38123 Povo, Trento, Italy
- ¹²⁴ Università degli Studi di Sassari, I-07100 Sassari, Italy
- ¹²⁵ INFN, Laboratori Nazionali del Sud, I-95125 Catania, Italy
- ¹²⁶ University of Portsmouth, Portsmouth, PO1 3FX, UK
- ¹²⁷ West Virginia University, Morgantown, WV 26506, USA
- ¹²⁸ The Pennsylvania State University, University Park, PA 16802, USA
- ¹²⁹ Physics and Astronomy Department, Stony Brook University, Stony Brook, NY 11794, USA
- ¹³⁰ Center for Computational Astrophysics, Flatiron Institute, 162 5th Ave, New York, NY 10010, USA
- ¹³¹ Colorado State University, Fort Collins, CO 80523, USA
- ¹³² Institute for Nuclear Research (Atomki), Hungarian Academy of Sciences, Bem tér 18/c, H-4026 Debrecen, Hungary
- ¹³³ CNR-SPIN, c/o Università di Salerno, I-84084 Fisciano, Salerno, Italy
- ¹³⁴ Scuola di Ingegneria, Università della Basilicata, I-85100 Potenza, Italy
- ¹³⁵ National Astronomical Observatory of Japan, 2-21-1 Osawa, Mitaka, Tokyo 181-8588, Japan
- ¹³⁶ Observatori Astronòmic, Universitat de València, E-46980 Paterna, València, Spain
- ¹³⁷ INFN Sezione di Torino, I-10125 Torino, Italy
- ¹³⁸ Indian Institute of Technology Bombay, Powai, Mumbai 400 076, India
- ¹³⁹ University of Szeged, Dóm tér 9, Szeged 6720, Hungary
- ¹⁴⁰ Delta Institute for Theoretical Physics, Science Park 904, 1090 GL Amsterdam, The Netherlands
- ¹⁴¹ Lorentz Institute, Leiden University, P.O. Box 9506, Leiden 2300 RA, The Netherlands
- ¹⁴² GRAPPA, Anton Pannekoek Institute for Astronomy and Institute for High-Energy Physics, University of Amsterdam, Science Park 904, 1098 XH Amsterdam, The Netherlands
- ¹⁴³ Tata Institute of Fundamental Research, Mumbai 400005, India
- ¹⁴⁴ INAF, Osservatorio Astronomico di Capodimonte, I-80131 Napoli, Italy
- ¹⁴⁵ University of Michigan, Ann Arbor, MI 48109, USA
- ¹⁴⁶ American University, Washington, D.C. 20016, USA
- ¹⁴⁷ University of California, Berkeley, CA 94720, USA
- ¹⁴⁸ Maastricht University, P.O. Box 616, 6200 MD Maastricht, The Netherlands
- ¹⁴⁹ Directorate of Construction, Services & Estate Management, Mumbai 400094, India
- ¹⁵⁰ University of Białystok, 15-424 Białystok, Poland
- ¹⁵¹ King's College London, University of London, London WC2R 2LS, UK
- ¹⁵² University of Southampton, Southampton SO17 1BJ, UK
- ¹⁵³ University of Washington Bothell, Bothell, WA 98011, USA
- ¹⁵⁴ Institute of Applied Physics, Nizhny Novgorod, 603950, Russia
- ¹⁵⁵ Ewha Womans University, Seoul 03760, Republic of Korea
- ¹⁵⁶ Inje University Gimhae, South Gyeongsang 50834, Republic of Korea
- ¹⁵⁷ National Institute for Mathematical Sciences, Daejeon 34047, Republic of Korea
- ¹⁵⁸ Ulsan National Institute of Science and Technology, Ulsan 44919, Republic of Korea
- ¹⁵⁹ Bard College, 30 Campus Rd, Annandale-On-Hudson, NY 12504, USA
- ¹⁶⁰ Chennai Mathematical Institute, Chennai 603103, India
- ¹⁶¹ NCBJ, 05-400 Świerk-Otwock, Poland
- ¹⁶² Institute of Mathematics, Polish Academy of Sciences, 00656 Warsaw, Poland
- ¹⁶³ Cornell University, Ithaca, NY 14850, USA
- ¹⁶⁴ Université de Montréal/Polytechnique, Montreal, Quebec H3T 1J4, Canada
- ¹⁶⁵ Lagrange, Université Côte d'Azur, Observatoire Côte d'Azur, CNRS, CS 34229, F-06304 Nice Cedex 4, France

- ¹⁶⁶ Hillsdale College, Hillsdale, MI 49242, USA
- ¹⁶⁷ Korea Astronomy and Space Science Institute, Daejeon 34055, Republic of Korea
- ¹⁶⁸ Institute for High-Energy Physics, University of Amsterdam, Science Park 904, 1098 XH Amsterdam, The Netherlands
- ¹⁶⁹ NASA Marshall Space Flight Center, Huntsville, AL 35811, USA
- ¹⁷⁰ University of Washington, Seattle, WA 98195, USA
- ¹⁷¹ Dipartimento di Matematica e Fisica, Università degli Studi Roma Tre, I-00146 Roma, Italy
- ¹⁷² INFN, Sezione di Roma Tre, I-00146 Roma, Italy
- ¹⁷³ ESPCI, CNRS, F-75005 Paris, France
- ¹⁷⁴ Center for Phononics and Thermal Energy Science, School of Physics Science and Engineering, Tongji University, 200092 Shanghai, People's Republic of China
- ¹⁷⁵ Southern University and A&M College, Baton Rouge, LA 70813, USA
- ¹⁷⁶ Department of Physics, University of Texas, Austin, TX 78712, USA
- ¹⁷⁷ Dipartimento di Fisica, Università di Trieste, I-34127 Trieste, Italy
- ¹⁷⁸ Centre Scientifique de Monaco, 8 quai Antoine Ier, MC-98000, Monaco
- ¹⁷⁹ Indian Institute of Technology Madras, Chennai 600036, India
- ¹⁸⁰ Université de Strasbourg, CNRS, IPHC UMR 7178, F-67000 Strasbourg, France
- ¹⁸¹ Institut des Hautes Etudes Scientifiques, F-91440 Bures-sur-Yvette, France
- ¹⁸² IISER-Kolkata, Mohanpur, West Bengal 741252, India
- ¹⁸³ Department of Astrophysics/IMAPP, Radboud University Nijmegen, P.O. Box 9010, 6500 GL Nijmegen, The Netherlands
- ¹⁸⁴ Kenyon College, Gambier, OH 43022, USA
- ¹⁸⁵ Whitman College, 345 Boyer Avenue, Walla Walla, WA 99362, USA
- ¹⁸⁶ Hobart and William Smith Colleges, Geneva, NY 14456, USA
- ¹⁸⁷ Department of Physics, Lancaster University, Lancaster LA1 4YB, UK
- ¹⁸⁸ OzGrav, Swinburne University of Technology, Hawthorn VIC 3122, Australia
- ¹⁸⁹ Trinity University, San Antonio, TX 78212, USA
- ¹⁹⁰ Dipartimento di Fisica, Università degli Studi di Torino, I-10125 Torino, Italy
- ¹⁹¹ Indian Institute of Technology, Gandhinagar Ahmedabad Gujarat 382424, India
- ¹⁹² INAF, Osservatorio Astronomico di Brera sede di Merate, I-23807 Merate, Lecco, Italy
- ¹⁹³ Centro de Astrofísica e Gravitação (CENTRA), Departamento de Física, Instituto Superior Técnico, Universidade de Lisboa, 1049-001 Lisboa, Portugal
- ¹⁹⁴ Marquette University, 11420 W. Clybourn St., Milwaukee, WI 53233, USA
- ¹⁹⁵ Indian Institute of Technology Hyderabad, Sangareddy, Khandi, Telangana 502285, India
- ¹⁹⁶ INAF, Osservatorio di Astrofisica e Scienza dello Spazio, I-40129 Bologna, Italy
- ¹⁹⁷ International Institute of Physics, Universidade Federal do Rio Grande do Norte, Natal RN 59078-970, Brazil
- ¹⁹⁸ Villanova University, 800 Lancaster Ave, Villanova, PA 19085, USA
- ¹⁹⁹ Andrews University, Berrien Springs, MI 49104, USA
- ²⁰⁰ Carleton College, Northfield, MN 55057, USA
- ²⁰¹ Department of Physics, Utrecht University, 3584CC Utrecht, The Netherlands
- ²⁰² Concordia University Wisconsin, 2800 N Lake Shore Dr, Mequon, WI 53097, USA

Received 2020 October 13; revised 2021 March 10; accepted 2021 March 10; published 2021 July 9

Abstract

We search for gravitational-wave transients associated with gamma-ray bursts (GRBs) detected by the Fermi and Swift satellites during the first part of the third observing run of Advanced LIGO and Advanced Virgo (2019 April 1 15:00 UTC–2019 October 1 15:00 UTC). A total of 105 GRBs were analyzed using a search for generic gravitational-wave transients; 32 GRBs were analyzed with a search that specifically targets neutron star binary mergers as short GRB progenitors. We find no significant evidence for gravitational-wave signals associated with the GRBs that we followed up, nor for a population of unidentified subthreshold signals. We consider several source types and signal morphologies, and report for these lower bounds on the distance to each GRB.

Unified Astronomy Thesaurus concepts: Gravitational waves (678); Gravitational wave astronomy (675); LIGO (920); Gamma-ray bursts (629); Compact binary stars (283); Neutron stars (1108); Black holes (162)

1. Introduction

Gamma-ray bursts (GRBs) are transient flashes of gamma radiation of cosmological origin observed at a rate of $\gtrsim 1$ per day (Nakar 2007). The interaction of matter with a compact central object, e.g., an accreting black hole (BH; Woosley 1993; Popham et al. 1999) or a magnetar (Usov 1992; Zhang & Meszaros 2001), is believed to drive highly relativistic jets which power the prompt emission of these astrophysical events. GRBs are broadly grouped into two classes—long and short GRBs—depending on the duration and spectral hardness of their prompt emission (Mazets et al. 1981; Norris et al. 1984; Kouveliotou et al. 1993).

Long, soft GRBs have durations $\gtrsim 2$ s and are firmly associated by optical observations to the collapse of massive stars

(Galama et al. 1998; Hjorth et al. 2003; Stanek et al. 2003; Hjorth & Bloom 2012). Gravitational waves (GWs) will be radiated by the core-collapse process, (e.g., Fryer & New 2011). Several models of this process do not yield radiation that is detectable by the current generation of GW interferometers beyond Galactic distances (Abbott et al. 2020c). However, rotational instabilities and instabilities induced by the additional presence of an accretion disk as part of the GRB engine may enhance the GW emission, making it detectable even for extragalactic sources (van Putten 2001; Davies et al. 2002; Fryer et al. 2002; Kobayashi & Meszaros 2003; Shibata et al. 2003; Piro & Pfahl 2007; Corsi & Meszaros 2009; Romero et al. 2010; Gossan et al. 2016; Abbott et al. 2020c).

The unambiguous association (Abbott et al. 2017a) of neutron star (NS) binary merger GW170817 (Abbott et al. 2017b, 2019d) and short GRB 170817A (Goldstein et al. 2017; Savchenko et al. 2017) has confirmed that compact binary mergers of this kind can

²⁰³ Please direct all correspondence to LSC Spokesperson at sc-spokesperson@ligo.org, or Virgo Spokesperson at virgo-spokesperson@ego-gw.it.

produce short GRBs. This milestone in multimessenger astronomy corroborated the idea first proposed in the 1980s (Blinnikov et al. 1984; Paczynski 1986; Eichler et al. 1989; Paczynski 1991; Narayan et al. 1992) that the progenitors of short GRBs are compact binaries containing NSs (for a review of proposed progenitors, see Lee & Ramirez-Ruiz 2007; Nakar 2007). Indirect evidence that had previously reinforced this idea was due to the observation of a possible kilonova associated with GRB 130603B (Berger et al. 2013; Tanvir et al. 2013), and to numerous studies of the environments of short GRBs (for reviews see Berger 2011, 2014), starting with the afterglow observation and host-galaxy association of GRB 050509B (Castro-Tirado et al. 2005; Gehrels et al. 2005; Bloom et al. 2006).

In addition to confirming the origin of *some* short GRBs, combining data from observations of GW170817 and GRB 170817A allowed for the inference of *basic* properties of short GRB jets. These include the isotropic equivalent luminosity of the jet, determined through a redshift measurement made possible by the optical follow-up of the GW localization (Abbott et al. 2017a; Goldstein et al. 2017), and the geometry of the GRB jets (Williams et al. 2018; Farah et al. 2020; Mogushi et al. 2019). The precise mechanism by which the jet is launched is still unknown, although it is typically believed to be either neutrino-driven or magnetically driven (Nakar 2007, but see also Liu et al. 2015 and references therein). Indeed, the scientific debate about the emission profile of the jet and the subsequent gamma-ray production mechanism of GRB 170817A is still ongoing (Hallinan et al. 2017; Kasliwal et al. 2017; Lamb & Kobayashi 2017; Troja et al. 2017; Gottlieb et al. 2018b; Lazzati et al. 2018; Gill & Granot 2018; Mooley et al. 2018; Zhang et al. 2018; Ghirlanda et al. 2019). It is generally believed that there are symmetric polar outflows of highly relativistic material that travel parallel to the total angular momentum of the binary system (Aloy et al. 2005; Kumar & Zhang 2014; Murguía-Berthier et al. 2017). These jets are thought to be collimated and roughly axisymmetric, emitting preferentially in a narrow opening angle due to a combination of outflow geometry and relativistic beaming. The data from extensive multi-wavelength observation campaigns that ran for nearly 20 months following the merger (Fong et al. 2019; Makhathini et al. 2020; Troja et al. 2020) are in agreement with a structured jet model, in which the energy and bulk Lorentz factor gradually decrease with angular distance from the jet symmetry axis (e.g., Dai & Gou 2001; Lipunov et al. 2001; Rossi et al. 2002; Zhang & Mészáros 2002; Ghirlanda et al. 2019; Beniamini et al. 2020). Further, according to one of the models proposed, as the jet drills through the surrounding merger ejecta it inflates a mildly relativistic cocoon due to interactions between the material at the edge of the jet and the ejecta (Lazzati et al. 2017; Gottlieb et al. 2018a). In this case, it is possible that the cocoon alone could produce the gamma-rays observed from GRB 170817A (Gottlieb et al. 2018b). Additional joint detections of GRBs and GWs will significantly aid our understanding of the underlying energetics (Lamb & Kobayashi 2017; Wu & MacFadyen 2018; Burns et al. 2019), jet geometry (Farah et al. 2020; Mogushi et al. 2019; Biscoveanu et al. 2020; Hayes et al. 2020), and jet ignition mechanisms (Veres et al. 2018; Ciolfi et al. 2019; Zhang 2019) of binary neutron star (BNS) coalescences.

A targeted search for GWs in sky and time coincidence with GRBs enhances our potential of achieving such joint detections. In this paper we present our results for the targeted GW follow-up of GRBs reported during the first part of the third observing run of Advanced LIGO and Advanced Virgo (O3a)

by the Fermi (Meegan et al. 2009) and Swift (Gehrels et al. 2004; Barthelmy et al. 2005) satellites. As in the first (Abbott et al. 2017c) and second (Abbott et al. 2017a, 2019b) observing runs, two searches with different assumptions about signal morphology are applied to the GW data: we process all GRBs with a search for generic GW transients (*X-Pipeline*; Sutton et al. 2010; Was et al. 2012, see Section 3.2 for details) and we follow up short GRBs with an additional, modeled search for BNS and neutron star–black hole (NSBH) GW inspiral signals (*PyGRB*; Harry & Fairhurst 2011; Williamson et al. 2014, see Section 3.1 for details). These searches were able to process 105 and 32 GRBs in O3a, respectively.

The scope of these targeted searches is to enhance our ability to detect GW signals in coincidence with GRBs with respect to all-sky searches for transient GW signals carried out by the LIGO Scientific & Virgo Collaboration (Abbott et al. 2019c, 2021). These may lead to joint GW–GRB detections in the case of loud GW events, as for GW170817 and GRB 170817A, but the targeted searches we report on here aim at uncovering subthreshold GW signals by exploiting the time and localization information of the GRBs themselves. The Fermi Gamma-ray Burst Monitor (GBM) team conducts an analogous effort when searching through GBM data for gamma-ray transients coincident with confirmed events and low-significance candidates reported by LIGO–Virgo offline analyses (Hamburg et al. 2020). Similarly, the Swift/Burst Alert Telescope (BAT) team has developed their own autonomous pipeline to enable subthreshold GRB searches for externally triggered events (Tohuvavohu et al. 2020).

This first part of the third observing run took place between 2019 April 1 15:00 UTC and 2019 October 1 15:00 UTC. Setting the false-alarm-rate threshold to two per year, 39 compact binary coalescence events were identified in O3a (Abbott et al. 2021). The majority of these have been classified as signals emitted by binary BH mergers; however, three events have the possibility of coming from a binary with at least one NS, that is, a potential short GRB progenitor.

1. GW190425 (Abbott et al. 2020a) was a compact binary coalescence with primary mass $2.0_{-0.3}^{+0.6}$ and secondary mass $1.4_{-0.3}^{+0.3}$ (all measurements quoted at the 90% credible level) and is therefore consistent with being the result of a BNS merger (Abbott et al. 2020a, 2021).
2. GW190426 was the GW candidate event with the highest false-alarm rate in Abbott et al. (2021); assuming it is a real signal, its inferred component masses of $5.7_{-2.3}^{+3.9}$ and $1.5_{-0.5}^{+0.8}$ indicate that it may have originated from an NSBH, or a binary BH merger.
3. GW190814 (Abbott et al. 2020b) could have originated from an NSBH, or a binary BH merger, as it has a primary mass measurement of $23.2_{-1.0}^{+1.1}$ and posterior support for a secondary mass $2.59_{-0.09}^{+0.08}$. This makes the secondary compact object either the lightest BH or the heaviest NS known to be in a compact binary system.

While there is considerable uncertainty in source type for all three of these events, GW190425 is the one for which the prospects of observing an associated GRB were most promising, as it is consistent with a BNS merger, rather than a binary BH merger or an NSBH merger with high or moderately high mass ratio. However, no confirmed electromagnetic or neutrino counterparts were observed in association with this event (Hosseinzadeh et al. 2019; Lundquist et al. 2019; Abbott et al. 2020a; Coughlin et al. 2020, 2020; see also

Pozanenko et al. 2020, 2020) despite extensive searches, which are logged in the Gamma-ray Coordinates Network (GCN) Circular archive.²⁰⁴ There are a number of reasons for which an electromagnetic counterpart associated with GW190425 may not have been detected. First, the large area covered by the localization region of GW190425 determined from GW data ($> 8000 \text{ deg}^2$) posed a considerable challenge for electromagnetic follow-up. 45.4% of this localization region was occulted by the Earth for the Fermi satellite so, if gamma-rays were emitted from the source, it is possible they were not detectable. Other gamma-ray observatories with lower sensitivities to short GRBs, such as INTEGRAL and KONUS-Wind, were covering relevant fractions of the localization region, however (Martin-Carrillo et al. 2019; Svinikin et al. 2019). Second, GRB jets are expected to be aligned with the total angular momentum of the binary system, and thus more easily detectable at small viewing angles. The binary inclination angle of GW190425 was poorly constrained, so it is possible that a jet from this system was formed but was oriented away from our line of sight. Additionally, the luminosity distance inferred for GW190425 ($\sim 160 \text{ Mpc}$) was significantly larger than that for GW170817 ($\sim 40 \text{ Mpc}$). GRB 170817A, which followed GW170817, was such an exceptionally faint short GRB (Abbott et al. 2017a) that its prompt emission photon flux would have dipped below the detection threshold for Fermi-GBM, had the source been farther than $\sim 75 \text{ Mpc}$ (Abbott et al. 2017a; Goldstein et al. 2017), and by $\sim 100 \text{ Mpc}$ it would become undetectable by Swift/BAT (Tohuvavohu et al. 2020). Thus, if emission from the system that produced GW190425 was similarly faint, it would not have been detectable by Swift/BAT or Fermi-GBM. Therefore, we do not necessarily expect a GRB detection to be associated with GW190425 due to its almost unconstrained inclination angle, large localization region, and distance, even if gamma-rays were emitted from this system. Scenarios like this one further motivate the need for GW follow-up analyses of GRB events which, by definition, constrain the sky localization and inclination angle of the progenitor.

In Section 2 we discuss the set of GRBs analyzed in this paper. In Section 3, we summarize the two targeted search methods used to follow up GRBs. Section 4 presents the results obtained with these two methods. We also consider each of the two sets of results collectively and quantify its consistency with the no-signal hypothesis. Finally, in Section 5 we provide our concluding remarks.

2. GRB Sample

The sample of GRBs analyzed in this paper includes events circulated by the GCN,²⁰⁵ complemented with information from the Swift/BAT catalog (Lien et al. 2016),²⁰⁶ the online Swift GRB Archive,²⁰⁷ and the Fermi-GBM Catalog.²⁰⁸ (Gruber et al. 2014; von Kienlin et al. 2014; Narayana Bhat et al. 2016) Once an alert detailing an event has been received via the GCN, the dedicated Vetting Automation and Literature Informed Database (Coyne 2015) is applied to find the latest

GRB results by comparing the time and localization parameters with those in tables relating to each satellite, the published catalogs, and an automatic literature search. The GCN notices provide a set of 141 GRBs during the O3a data-taking period (2019 April 1 15:00 UTC–2019 October 1 15:00 UTC).

As mentioned in the Introduction, we carry out two searches with distinct assumptions about signal morphology (see Section 3 for details on both methods): a search for generic GW transients and a modeled search for GW signals from NS binary inspirals, i.e., BNSs and NSBHs. We do this because GRBs of different durations are expected to have different origins and therefore different GW signal morphologies. In particular, if a compact binary merger were to produce a GRB it would be expected to have a short duration. In order to specifically target such phenomena with the modeled search, we classify each GRB as *long*, *short*, or *ambiguous*. This classification relies on the measurement of the time interval over which 90% of the total background-subtracted photon counts are observed (T_{90} , with error $|\delta T_{90}|$). When $T_{90} + |\delta T_{90}| < 2 \text{ s}$ the GRBs are labeled as short, when $T_{90} - |\delta T_{90}| > 4 \text{ s}$ the GRBs are labeled as long, and the rest are labeled as ambiguous. The unmodeled search for generic transients is applied to GRBs of all classifications. All of the short and ambiguous GRBs are additionally analyzed with the modeled search in order to maximize the chances of uncovering any potential binary coalescence candidate.

The classification process results in 20 short GRBs, 108 long GRBs, and 13 ambiguous GRBs. As in Abbott et al. (2019b), we require a minimum amount of coincident data from at least two GW detectors around the time of a GRB for the generic unmodeled GW transient search to assess the significance of a GW candidate with sub-percent level accuracy (see Section 3.2 for technical details). This requirement is applied to GRBs of all classifications and results in 105 GRBs being analyzed with this method, out of the 141 GRBs recorded by Fermi and Swift during O3a. This amounts to 74.5%, a percentage of events that is compatible with the fraction of observing time during which at least two interferometers in the network were operating in observing mode (81.9%; Abbott et al. 2021). Similarly, requirements from the modeled search (see Section 3.1 for technical details) set the minimum amount of data needed from at least one detector around the time of the GRBs. It leads to 32 short and ambiguous GRBs being analyzed with this method,²⁰⁹ that is, 97.0% of the 33 possible ones. This value matches the fraction of observing time during which at least one interferometer in the network was operating in observing mode during O3a (96.9%; Abbott et al. 2021).

Of the 141 Fermi and Swift GRBs in our sample, the vast majority do not have redshift measurements. Those that do are the ambiguous GRB 190627A at $z = 1.942$ (Japelj et al. 2019), and the two long GRBs 190719C and 190829A at $z = 2.469$ and $z = 0.0785$, respectively (Rossi et al. 2019; Valeev et al. 2019). All three fall beyond the detection range of our interferometers, and are not expected to produce measurable GW results. Regardless of availability of redshift information,

²⁰⁹ The single GRB we were unable to follow up with the modeled search is GRB 190605974. The GRBs we were unable to analyze with either of the searches are: GRB 190401139, GRB 190406745, GRB 190411407, GRB 190422A, GRB 190424A, GRB 190508808, GRB 190515B, GRB 190530430, GRB 190531840, GRB 190604B, GRB 190605974, GRB 190607071, GRB 190609315, GRB 190611A, GRB 190611950, GRB 190622368, GRB 190626254, GRB 190706B, GRB 190714573, GRB 190716917, GRB 190719113, GRB 190723309, GRB 190731943, GRB 190804792, GRB 190806675, GRB 190808498, GRB 190814837, GRB 190821A, GRB 190821716, GRB 190828614.

²⁰⁴ All GCN Circulars related to this event are archived at <https://gcn.gsfc.nasa.gov/other/S190425z.gcn3>.

²⁰⁵ GCN Circulars Archive: http://gcn.gsfc.nasa.gov/gcn3_archive.html.

²⁰⁶ Swift/BAT GRB Catalog: <http://swift.gsfc.nasa.gov/results/batgrbcatalog/>.

²⁰⁷ Swift GRB Archive: http://swift.gsfc.nasa.gov/archive/grb_table/.

²⁰⁸ FERMIGBRST—Fermi-GBM Burst Catalog: <https://heasarc.gsfc.nasa.gov/W3Browse/fermi/fermigbrst.html>.

however, we followed up as many GRBs as we could and we were indeed able to analyze these three cases.

3. Search Methods

We now provide a description of the two targeted search methods used in this paper. These are the same methods applied to GW data coincident with GRBs that occurred during the first (Abbott et al. 2017c) and second (Abbott et al. 2017a, 2019b) Advanced LIGO and Virgo observing runs. In Section 3.1 we summarize the modeled search method that aims at uncovering subthreshold GW signals emitted by BNS and NSBH binaries (PyGRB; Harry & Fairhurst 2011; Williamson et al. 2014). In Section 3.2 we discuss the search for generic GW transients (X-Pipeline; Sutton et al. 2010; Was et al. 2012). Results from these two searches are presented in Section 4.

3.1. Modeled Search for Binary Mergers

This analysis searches for a GW signal compatible with the inspiral of a BNS or NSBH binary—collectively NS binaries—within 6 s of data associated with an observed short GRB. This stretch of data is the *on-source window* and runs from -5 s to $+1$ s around the start of the GRB emission (i.e., the GRB trigger time). The surrounding ~ 30 – 90 minutes of data are split into 6 s *off-source trials* which are also analyzed in order to build a background. Around 30 minutes allows the modeled search to accurately estimate the power spectral density of the available instruments and ensures that it can assess at sub-percent level accuracy the significance of any candidate events found in the on-source window. All the data are processed using PyGRB (Harry & Fairhurst 2011; Williamson et al. 2014), a coherent matched filtering pipeline that is part of the general open-source software PyCBC (Nitz et al. 2020) and has core elements in the LALSuite software library (LIGO Scientific Collaboration 2018). We scan each trial of data and the on-source window in the 30–1000 Hz frequency band using a predefined bank of waveform templates (Owen & Sathyaprakash 1999) created with a hybrid geometric–stochastic method (Capano et al. 2016; Dal Canton & Harry 2017) and using a phenomenological inspiral–merger–ringdown waveform model for non-precessing point-particle binaries (IMRPhenomD; Husa et al. 2016; Khan et al. 2016).²¹⁰ The waveform template bank includes waveforms corresponding to a range of masses ($[1.0, 2.8]M_{\odot}$ for NSs, $[1.0, 25.0]M_{\odot}$ for BHs) and dimensionless spin magnitudes ($[0, 0.05]$ for NSs, $[0, 0.998]$ for BHs) for aligned-spin, zero-eccentricity BNS or NSBH systems that may produce an electromagnetic counterpart via the tidal disruption of the NS (Pannarale & Ohme 2014). Aside from the updated sensitivity of our detectors, the only difference with respect to the second LIGO–Virgo observing run (Abbott et al. 2019b) is that the generation of the bank has been updated to apply more accurate physics to determine whether an NSBH system could produce an accretion disk from this disruption (Foucart et al. 2018). We only search for circularly polarized GWs, which may be emitted by binaries with inclinations of 0° or 180° : such systems have GW amplitudes that are consistent (Williamson et al. 2014) with those of binary progenitors with inclination angles over the full range of viewing angles that we expect for typical brightness GRBs ($\lesssim 30^{\circ}$; Fong et al. 2015), such as those in our sample.

The strength of any potential signal is ranked via a coherent matched filter signal-to-noise ratio (S/N; Harry & Fairhurst 2011; Williamson et al. 2014) which is re-weighted according to a χ^2 goodness-of-fit between the template that identified it and the signal itself. The significance of the latter is quantified as the probability of background alone producing such an event. This is evaluated by comparing the re-weighted S/N of the loudest trigger within the 6 s on-source to the distribution of the re-weighted S/Ns of the loudest triggers in the 6 s off-source trials. When data from more than one detector are available, this background S/N distribution is extended by generating additional off-source trials via *time slides*, that is, by combining data from detectors after introducing time shifts longer than the light-travel time across the network. Specifically, our time shifts are 6 s long, in order to match the width of the on-source window and the off-source trials.

In order to derive the sensitivity of this search to potential GRB sources, simulated signals are injected in software into the off-source data. The 90% exclusion distances, D_{90} , are defined as the distances within which 90% of the injected simulated signals are recovered with a greater ranking statistic than the loudest on-source event. Three different astrophysical populations are considered: BNS binaries with generically oriented—i.e., precessing—spins, aligned-spin NSBH binaries, and NSBH binaries with generically oriented spins. These simulated signals cover a portion of parameter space that extends beyond that covered by the template bank, as they include NS dimensionless spin values up to 0.4 and, for two families of injected signals, admit precession. As stated previously, the templates used to filter the data are produced using IMRPhenomD. In order to factor into the sensitivity assessment any potential loss due to uncertainties in GW signal modeling, the injected signals are not produced with the same model used for the templates. Precessing BNS signals are simulated using the TaylorT2 time-domain, post-Newtonian inspiral approximant (SpinTaylorT2; Sathyaprakash & Dhurandhar 1991; Blanchet et al. 1996; Mikoczi et al. 2005; Arun et al. 2009; Bohé et al. 2013, 2015; Mishra et al. 2016), while NSBH-injected waveforms are generated assuming a point-particle effective-one-body model tuned to numerical simulations which can allow for precession effects from misaligned spins (SEOBNRv3; Pan et al. 2014; Taracchini et al. 2014; Babak et al. 2017). The three populations used to build the injected signals are defined as in the first two LIGO–Virgo observing runs, to allow for direct comparisons (Abbott et al. 2017c, 2019b). NS masses for the injections are taken between $1 M_{\odot}$ and $3 M_{\odot}$ from a normal distribution centered at $1.4 M_{\odot}$ with a standard deviation of $0.2 M_{\odot}$ (Kiziltan et al. 2013) and $0.4 M_{\odot}$ for BNS and NSBH systems, respectively. BH masses are taken to be between $3 M_{\odot}$ and $15 M_{\odot}$ from a normal distribution centered at $10 M_{\odot}$ with a standard deviation of $6 M_{\odot}$. Spins are drawn uniformly in magnitude and, when applicable, with random orientation; the maximum allowed NS spin magnitude is 0.4, from the fastest observed pulsar spin (Hessels et al. 2006), while the maximum BH spin magnitude is set to 0.98, motivated by X-ray binary observations (e.g., Özel et al. 2010; Kreidberg et al. 2012; Miller & Miller 2014). Injected signals have a range of total inclinations from 0° – 30° and 150° – 180° while removing any systems which could not feasibly produce a short GRB (Pannarale & Ohme 2014).

3.2. Unmodelled Search for Generic Transients

X-Pipeline looks for excess power that is coherent across the network of GW detectors and consistent with the sky

²¹⁰ All waveforms mentioned in this section are generated with the LALSimulation package that is part of the LALSuite software library (LIGO Scientific Collaboration 2018).

localization and time window for each GRB. As in the first two observing runs, we use a search time window that begins 600 s before the GRB trigger time and ends 60 s after it, or at the T_{90} time itself (whichever is larger). This window is long enough to encapsulate the time delay between GW emission from a progenitor and the GRB prompt emission (Koshut et al. 1995; Aloy et al. 2000; MacFadyen et al. 2001; Zhang et al. 2003; Lazzati 2005; Wang & Meszaros 2007; Burlon et al. 2008, 2009; Lazzati et al. 2009; Vedrenne & Atteia 2009). Our frequency range is restricted to the most sensitive band of the GW detectors, namely 20–500 Hz. While gravitational radiation from core-collapse supernovae is expected to contain frequency content above this band (Radice et al. 2019), detection of bursts above a few hundred hertz is not energetically favorable (see, e.g., Figure 4 in Abbott et al. 2019a) and increasing the frequency upper limit also increases the computational cost.

The generic transient search pipeline coherently combines data from all detectors and produces time–frequency maps of this GW data stream. The maps are scanned for clusters of pixels with excess energy, referred to as *events*. The events obtained this way are first ranked according to a detection statistic based on energy and then subject to coherent consistency tests. These are based on correlations between data in different detectors and reject events associated with noise transients. The surviving event with the largest ranking statistic is taken to be the best candidate for a GW detection. Its significance is evaluated in the same way as in the modeled analysis, but with 660 s long off-source trials. In order to ensure that the significance is assessed at a sub-percent level, we require at least ~ 1.5 hr of coincident data from at least two detectors around the time of a GRB. Non-Gaussian noise transients, or *glitches*, are handled as described in Abbott et al. (2019b).

Similarly to the modeled search, we quantify the sensitivity of the generic transient search by injecting simulated signals into off-source data in software and recovering them. Calibration errors are accounted for by jittering the amplitude and arrival time of the injections according to a Gaussian distribution representative of the calibration uncertainties in O3a (Abbott et al. 2017c). We report results obtained for four distinct sets of circular sine-Gaussian (CSG) waveforms, with fixed quality factor $Q=9$ and with central frequencies of 70, 100, 150, and 300 Hz (see Equation (1) and Section 3.2 of Abbott et al. 2017c). These models are intended to represent the GWs from stellar collapses. In all four cases, we set the total radiated energy to $E_{\text{GW}} = 10^{-2} M_{\odot} c^2$, a choice that is about an order of magnitude higher than the results presented in Abbott et al. (2020c) for the detectability of core-collapse supernovae. As optimistic representatives (Ott & Santamaría 2013) of longer-duration GW signals detectable by the unmodeled search, we use accretion disk instability (ADI) waveforms (van Putten 2001; van Putten et al. 2014). In these ADI models, instabilities form in a magnetically suspended torus around a rapidly spinning BH, causing GWs to be emitted. The model specifics and parameters used to generate the five families of ADI signals that we consider are the same as in Table 1 and Section 3.2 of Abbott et al. (2017c).

4. Results

During O3a we used the generic transient method to follow up a total of 105 GRBs, whereas the modeled search was applied to the 32 GRB triggers classified as short or ambiguous. For all of the

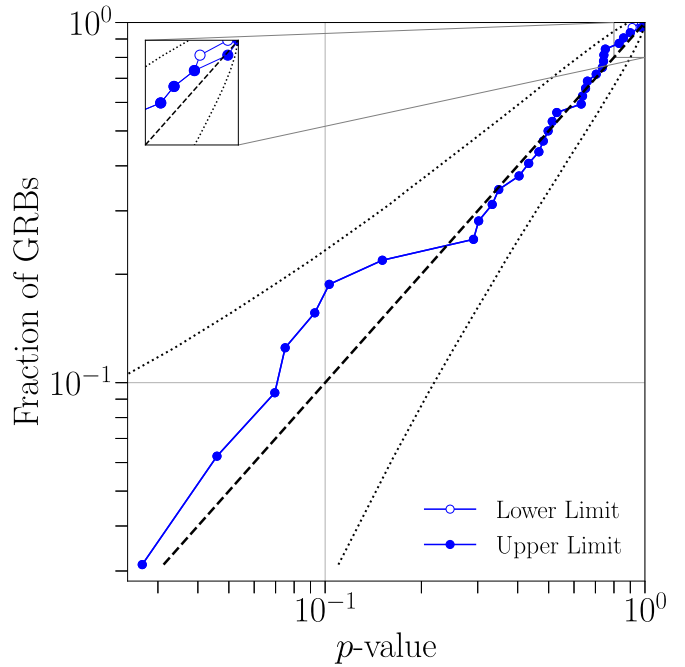


Figure 1. Cumulative distribution of loudest on-source event p -values for the neutron star binary modeled search in O3a. If the search reports no trigger in the on-source, we plot an upper limit on the p -value of 1 (open circles), and a lower limit equal to the fraction of off-source trials that contained no trigger (full circles). The dashed line indicates the expected distribution of p -values under the no-signal hypothesis, with the corresponding 2σ envelope marked by dotted lines.

most GW-signal-like triggers associated with the examined GRBs, the searches returned no significant probability of incompatibility with background alone (p -value). This indicates that no GW signal was uncovered in association with any of these GRBs. This is consistent with the estimated GW–GRB joint detection rate with Fermi-GBM of 0.07–1.80 per year reported in Abbott et al. (2019b) for the 2019–2020 LIGO–Virgo observing run. The most significant events found by the generic transient method and by the modeled search had p -values of 5.5×10^{-3} (GRB 190804058) and 2.7×10^{-2} (GRB 190601325), respectively.

Figures 1 and 2 show the cumulative distributions of p -values returned by the modeled search and the generic transient search, respectively. For cases in which no associated on-source trigger survived the analysis cuts of the modeled search, the associated p -value ranges between 1—i.e., an upper bound on a probability—and the fraction of background trials for the GRB that also yielded no associated GW trigger. In both figures, the expected background distribution under the no-signal hypothesis is shown by the dashed line, and its 2σ limits are indicated by the two dotted lines. Both cumulative distributions are within the 2σ lines and therefore compatible with the no-signal hypothesis. These figures indicate that the lowest p -value found by each search is compatible with the no-signal hypothesis.

Having found no GW signal associated with the GRBs followed up by our searches, we consider the set of modeled search results and the set of generic transient search results, collectively. We apply a weighted binomial test described in Abadie et al. (2012) to evaluate how consistent each set of results is collectively with the no-signal hypothesis. This test is conducted using the most significant 5% of p -values in the sample weighted by a prior probability of detection estimated

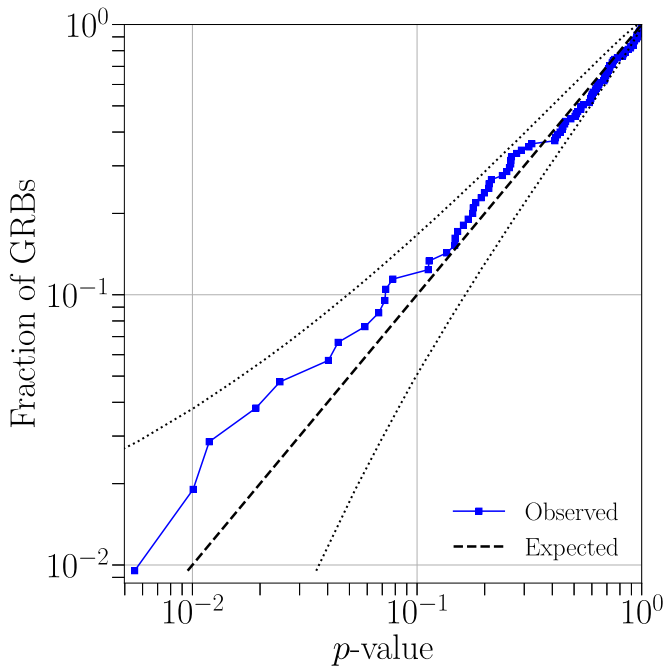


Figure 2. Cumulative distribution of p -values from the unmodelled search for transient gravitational waves associated with 105 gamma-ray bursts. The dashed line represents the expected distribution under the no-signal hypothesis, with dotted lines indicating a 2σ deviation from this distribution.

using the network detector sensitivity at the time and location of each GRB. This final probability of observing this distribution of p -values given background alone, i.e., under the no-signal hypothesis, was 0.43 (0.31) for the modeled (generic transient) search method. Therefore, both searches gave no significant evidence for a population of unidentified subthreshold GW signals. For the analyses carried out in the first observing run of Advanced LIGO and Advanced Virgo, the combined p -values were 0.57 and 0.75 for the modeled and generic transient search, respectively (Abbott et al. 2017c); in the second observing run of Advanced LIGO and Advanced Virgo, they were 0.30 and 0.75 (Abbott et al. 2019b).

In Figure 3, we show the cumulative 90% exclusion distances for the 32 short and ambiguous GRBs followed up with the modeled search. The lowest exclusion distance values (~ 20 Mpc) were obtained for ambiguous GRB 190409901. This is due to the fact that only Virgo data were available for this GRB and that the sky location of this event was in a direction in which Virgo had $\sim 30\%$ sensitivity with respect to an optimal sky location. For each of the three simulated signal classes, we quote the median of the 32 D_{90} results in the top part of Table 1. All three values are 40%–60% times higher than those reported in Abbott et al. (2019b) for the previous LIGO–Virgo observing run. The individual D_{90} values for each class of simulated signals are reported in Table 2. As a term of comparison, during the six month duration of O3a, the Hanford and Livingston Advanced LIGO instruments, and the Virgo interferometer had BNS ranges of 108 Mpc, 135 Mpc, and 45 Mpc, respectively.²¹¹ We also place a 90% confidence level lower limit on the distance for each of the 105 GRBs analyzed by the generic transient search, assuming the various emission

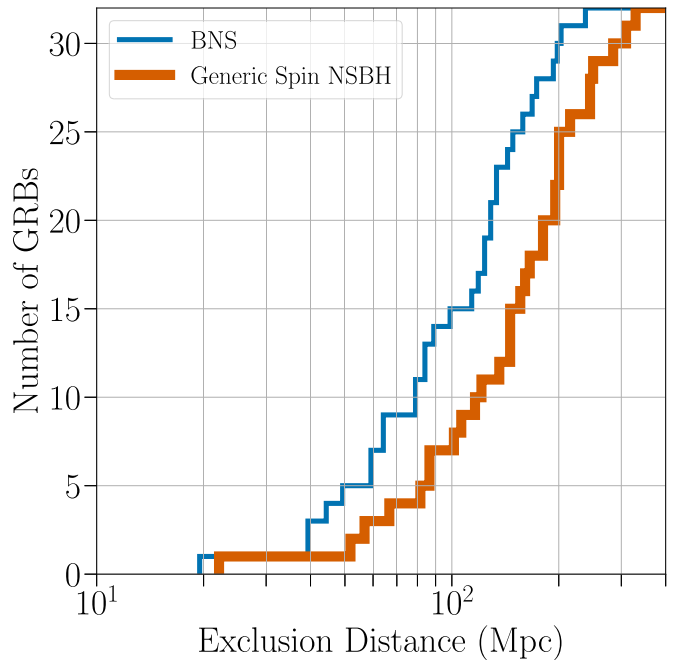


Figure 3. Cumulative histograms of the 90% confidence exclusion distances, D_{90} , for the binary neutron star (blue, thin line) and generically spinning neutron star–black hole (orange, thick line) signal models, shown for the sample of 32 short and ambiguous gamma-ray bursts (GRBs) that were followed up by the NS binary modeled search during O3a, none of which had an identified gravitational wave counterpart. For a given GRB event and signal model, D_{90} is the distance within which 90% of simulated signals inserted into off-source data are recovered with greater significance than the most significant on-source trigger. These simulated signals have inclinations θ_{JN} —the angle between the total angular momentum and the line of sight—drawn uniformly in $\sin \theta_{JN}$ with θ_{JN} restricted to $[0^\circ, 30^\circ] \cup [150^\circ, 180^\circ]$.

Table 1
Median 90% Confidence Level Exclusion Distances, D_{90} , for the Searches during O3a

Modelled Search (Short GRBs)	NSBH		NSBH	
	BNS	Generic Spins	Aligned Spins	
D_{90} [Mpc]	119	160	231	
Unmodelled search (All GRBs)	CSG	CSG	CSG	CSG
	70 Hz	100 Hz	150 Hz	300 Hz
D_{90} (Mpc)	146	104	73	28
Unmodelled search (All GRBs)	ADI	ADI	ADI	ADI
	A	B	C	D
D_{90} (Mpc)	23	123	28	11

Note. Modeled search results are shown for three classes of NS binary progenitor model, and unmodeled search results are shown for CSG (Abbott et al. 2017c) and ADI (van Putten 2001; van Putten et al. 2014) models.

models discussed in Section 3.2 (see also Abbott et al. 2017c). Figure 4 shows the distribution of D_{90} values for the ADI model A (van Putten 2001; van Putten et al. 2014) and for a CSG with central frequency of 150 Hz (Abbott et al. 2017c). These limits depend on the sensitivity of the detector network which, in turn, varies over time and with sky location, and have been marginalized over errors introduced by detector calibration. For the ADI and the CSG models mentioned above, as well as for the other seven models used in the generic transient

²¹¹ The BNS inspiral range is defined as the distance at which the coalescence of two $1.4 M_{\odot}$ NSs can be detected with an S/N of 8, averaged over all directions in the sky, source orientation, and polarization (Finn & Chernoff 1993; Allen et al. 2012; Chen et al. 2021).

Table 2
Information and Limits on Associated GW Emission for Each of the Fermi and Swift GRBs Followed Up during the LIGO–Virgo Run O3a

GRB Name	UTC Time	R.A.	Decl.	Satellite	Type	Network	D_{90} (Mpc)				
							BNS	Generic NSBH	Aligned NSBH	ADI-A	CSG 150 Hz
190404293	07:01:21	8 ^h 05 ^m 33 ^s	55° 25′	Fermi	Long	HIL1	35	152
190406450	10:47:20	23 ^h 46 ^m 21 ^s	20° 23′	Fermi	Long	HIL1V1	2	115
190406465	11:09:47	19 ^h 05 ^m 21 ^s	61° 30′	Fermi	Long	HIL1V1	69	186
190407575	13:48:36	6 ^h 02 ^m 07 ^s	−64° 08′	Fermi	Long	HIL1V1 [†]	61	171
190407672	16:07:26	12 ^h 07 ^m 16 ^s	40° 37′	Fermi	Long	L1V1	32	49
190407788	18:54:41	13 ^h 30 ^m 57 ^s	−7° 57′	Fermi	Ambiguous	L1V1	169	311	395	34	54
190409901	21:38:05	15 ^h 19 ^m 53 ^s	−33°52′	Fermi	Ambiguous	V1	19	22	34
190411579	13:53:58	3 ^h 02 ^m 31 ^s	48° 38′	Fermi	Long	HIL1V1 [†]	10	108
190415173	04:09:49	1 ^h 50 ^m 50 ^s	17° 26′	Fermi	Long	H1V1	2	5
190419414	09:55:37	7 ^h 05 ^m 48 ^s	−40° 08′	Fermi	Long	H1V1 [†]	34	54
190420981	23:32:24	21 ^h 17 ^m 09 ^s	−66° 25′	Fermi	Ambiguous	L1V1	175	215	315	35	52
190422284	06:48:17	20 ^h 26 ^m 38 ^s	−73° 01′	Fermi	Long	HIL1 [†]	14	127
190422670	16:05:04	12 ^h 36 ^m 55 ^s	−54° 57′	Fermi	Long	HIL1V1	2	167
190425089	02:07:43	21 ^h 01 ^m 43 ^s	−15° 13′	Fermi	Ambiguous	L1V1(HIL1)	204	247	440	23	38
190427A	04:34:15	18 ^h 40 ^m 52 ^s	40° 19′	Swift	Short	L1V1	138	199	253	33	92
190428783	18:48:12	1 ^h 55 ^m 45 ^s	15° 51′	Fermi	Long	L1V1	29	38
190429743	17:49:50	13 ^h 20 ^m 12 ^s	−7° 60′	Fermi	Long	HIL1V1	70	126
190501794	19:03:42	10 ^h 25 ^m 09 ^s	−22° 00′	Fermi	Long	L1V1 [†]	18	35
190502168	04:01:30	6 ^h 16 ^m 43 ^s	3° 17′	Fermi	Long	HIL1V1	34	92
190504415	09:57:34	4 ^h 41 ^m 57 ^s	39° 34′	Fermi	Long	HIL1V1 [†]	16	50
190504678	16:16:28	9 ^h 09 ^m 43 ^s	33° 01′	Fermi	Short	L1V1	93	124	189	17	68
190505051	01:14:09	22 ^h 21 ^m 33 ^s	42° 11′	Fermi	Short	L1V1	100	149	206	24	36
190507270	06:28:23	10 ^h 23 ^m 50 ^s	−12° 48′	Fermi	Long	HIL1 [†]	39	111
190507712	17:05:16	05 ^h 44 ^m 53 ^s	−61°7′	Fermi	Short	V1	42	58	70
190507970	23:16:29	19 ^h 11 ^m 16 ^s	−22° 49′	Fermi	Long	HIL1V1	32	231
190508987	23:41:24	6 ^h 54 ^m 02 ^s	27° 02′	Fermi	Long	HIL1V1 [†]	30	178
190510120	02:52:13	8 ^h 18 ^m 09 ^s	−53° 04′	Fermi	Long	H1V1 [†]	8	53
190510430	10:19:16	8 ^h 32 ^m 31 ^s	33° 33′	Fermi	Short	HIL1	128	196	253	48	116
190511A	07:14:48	8 ^h 25 ^m 46 ^s	−20° 15′	Swift	Long	HIL1	50	142
190512A	14:40:09	5 ^h 29 ^m 35 ^s	−7° 35′	Swift	Long	L1V1	20	56
190515190	04:33:03	9 ^h 10 ^m 45 ^s	29° 17′	Fermi	Short	L1V1	122	148	194	22	42
190517813	19:30:10	18 ^h 00 ^m 04 ^s	25° 46′	Fermi	Long	HIL1	30	74
190519A	07:25:39	7 ^h 39 ^m 01 ^s	−38° 49′	Swift	Long	HIL1V1	10	190
190525032	00:45:47	22 ^h 32 ^m 04 ^s	5° 27′	Fermi	Short	HIL1V1	128	248	385	22	165
190531312	07:29:11	1 ^h 24 ^m 28 ^s	16° 21′	Fermi	Long	L1V1	21	73
190531568	13:38:03	18 ^h 16 ^m 40 ^s	38° 52′	Fermi	Short	H1V1	86	150	187	3	29
190601325	07:47:24	10 ^h 51 ^m 55 ^s	54° 35′	Fermi	Short	H1V1	136	169	248	17	34
						(HIL1V1)					
190603795	19:04:25	1 ^h 20 ^m 19 ^s	40° 55′	Fermi	Long	HIL1	3	156
190604446	10:42:37	22 ^h 50 ^m 12 ^s	46° 22′	Fermi	Long	HIL1	72	174
190606080	01:55:07	5 ^h 06 ^m 09 ^s	−0° 41′	Fermi	Short	H1V1	52	68	81	8	37
190608009	00:12:18	15 ^h 02 ^m 57 ^s	−31° 25′	Fermi	Long	L1V1 [†]	15	30
190610750	17:59:49	21 ^h 49 ^m 31 ^s	42° 25′	Fermi	Long	L1V1	1	40
190610834	20:00:23	20 ^h 59 ^m 19 ^s	−15° 56′	Fermi	Ambiguous	L1V1	149	202	306	34	58
190610A	11:27:45	3 ^h 04 ^m 57 ^s	−7° 40′	Swift	Short	HIL1	63	82	114	23	58
190612165	03:57:24	14 ^h 55 ^m 48 ^s	62° 06′	Fermi	Long	HIL1V1 [†]	48	178
190613A	04:07:18	12 ^h 10 ^m 12 ^s	67° 15′	Swift	Long	HIL1V1	70	200
190613B	10:47:02	20 ^h 21 ^m 45 ^s	−4° 39′	Swift	Long	HIL1 [†]	54	160
190615636	15:16:27	12 ^h 45 ^m 36 ^s	49° 23′	Fermi	Long	HIL1V1	4	45
190619018	00:26:01	23 ^h 17 ^m 14 ^s	12° 52′	Fermi	Long	HIL1V1 [†]	6	132
190619595	14:16:25	19 ^h 24 ^m 16 ^s	20° 10′	Fermi	Long	HIL1V1 [†]	2	47
190620507	12:10:10	10 ^h 48 ^m 19 ^s	30° 29′	Fermi	Long	HIL1	5	94
190623461	11:03:27	22 ^h 21 ^m 57 ^s	−23° 20′	Fermi	Long	HIL1V1	10	95
190627481	11:31:59	23 ^h 29 ^m 02 ^s	−8° 53′	Fermi	Long	HIL1	16	116
190627A	11:18:31	16 ^h 19 ^m 29 ^s	−5° 18′	Swift	Ambiguous	HIL1	115	139	211	21	77
190628521	12:30:55	9 ^h 36 ^m 19 ^s	−77° 04′	Fermi	Long	HIL1	47	164
190630257	06:09:58	20 ^h 27 ^m 55 ^s	−1° 20′	Fermi	Short	H1V1	47	91	121	16	25
190630B	06:02:08	14 ^h 54 ^m 55 ^s	41° 32′	Swift	Long	H1V1	10	12
190630C	23:52:59	19 ^h 35 ^m 33 ^s	−32° 46′	Swift	Long	HIL1V1	47	118
190701A	09:45:20	1 ^h 52 ^m 31 ^s	58° 54′	Swift	Long	HIL1V1	12	157
190707285	06:50:05	10 ^h 11 ^m 28 ^s	−30° 59′	Fermi	Long	HIL1V1	49	163

Table 2
(Continued)

GRB Name	UTC Time	R.A.	Decl.	Satellite	Type	Network	D_{90} (Mpc)				
							BNS	Generic NSBH	Aligned NSBH	ADI-A	CSG 150 Hz
190707308	07:23:01	12 ^h 17 ^m 19 ^s	−9° 31′	Fermi	Long	HIL1	34	75
190708365	08:45:11	13 ^h 59 ^m 24 ^s	−1° 18′	Fermi	Long	HIL1V1	18	58
190712018	00:25:20	22 ^h 44 ^m 14 ^s	−38° 35′	Fermi	Ambiguous	HIL1	68	204	357
190712095	02:16:41	19 ^h 13 ^m 33 ^s	56° 09′	Fermi	Long	HIL1V1	38	159
190716019	00:27:59	4 ^h 41 ^m 40 ^s	16° 28′	Fermi	Long	HIL1 [†]	5	12
190718A	04:41:15	22 ^h 26 ^m 25 ^s	−41° 11′	Swift	Long	HIL1 [†]	12	93
190719499	11:57:51	6 ^h 34 ^m 26 ^s	6° 42′	Fermi	Long	HIL1V1	33	94
190719C	14:58:34	16 ^h 00 ^m 49 ^s	13° 00′	Swift	Long	HIL1V1 [†]	4	157
190720613	14:42:09	13 ^h 30 ^m 52 ^s	41° 47′	Fermi	Long	HIL1V1	10	38
190720964	23:08:38	9 ^h 15 ^m 28 ^s	−55° 35′	Fermi	Long	HIL1	10	34
190724031	00:43:56	11 ^h 21 ^m 24 ^s	15° 9′	Fermi	Short	HIL1	197	286	329
190726642	15:24:53	20 ^h 41 ^m 02 ^s	34° 17′	Fermi	Long	HIL1V1 [†]	34	85
190726843	20:14:30	22 ^h 50 ^m 43 ^s	−55° 59′	Fermi	Long	HIL1V1 [†]	72	180
190727668	16:01:52	14 ^h 57 ^m 57 ^s	19° 26′	Fermi	Long	HIL1	24	109
190727B	20:18:17	8 ^h 25 ^m 59 ^s	−13° 16′	Swift	Long	L1V1	34	68
190728271	06:30:36	23 ^h 46 ^m 45 ^s	5° 26′	Fermi	Short	HIL1V1	160	204	272	32	79
190804058	01:23:27	7 ^h 12 ^m 04 ^s	−64° 52′	Fermi	Ambiguous	H1V1	132	184	240	34	74
190805106	02:32:30	11 ^h 10 ^m 36 ^s	−23° 46′	Fermi	Long	HIL1V1	35	121
190805199	04:46:00	13 ^h 59 ^m 00 ^s	19° 28′	Fermi	Long	H1V1	33	75
190806535	12:50:02	20 ^h 22 ^m 14 ^s	0° 33′	Fermi	Long	HIL1V1	20	52
190808752	18:03:17	11 ^h 12 ^m 12 ^s	39° 43′	Fermi	Long	L1V1	32	62
190810675	16:12:01	12 ^h 55 ^m 07 ^s	−37° 34′	Fermi	Short	HIL1V1	85	159	222	2	50
190813520	12:29:09	7 ^h 05 ^m 31 ^s	−23° 16′	Fermi	Short	HIL1	84	121	161	23	56
190816A	14:42:24	22 ^h 44 ^m 43 ^s	−29° 45′	Swift	Long	L1V1 [†]	34	75
190817953	22:52:25	18 ^h 20 ^m 40 ^s	−31° 08′	Fermi	Ambiguous	HIL1	61	102	109	1	30
190822705	16:55:29	8 ^h 49 ^m 04 ^s	−8° 05′	Fermi	Short	L1V1	148	181	278	2	17
190824A	14:46:39	14 ^h 21 ^m 17 ^s	−41° 54′	Swift	Long	HIL1V1 [†]	24	160
190825171	04:06:56	14 ^h 03 ^m 26 ^s	−74° 08′	Fermi	Long	L1V1	17	38
190827467	11:12:48	11 ^h 43 ^m 14 ^s	46° 27′	Fermi	Long	HIL1	7	26
190828B	12:59:59	16 ^h 47 ^m 21 ^s	27° 17′	Swift	Long	H1V1 [†]	22	52
190829A	19:56:44	2 ^h 58 ^m 10 ^s	−8° 57′	Swift	Long	L1V1 [†]	33	51
190830023	00:32:48	7 ^h 27 ^m 36 ^s	−23° 46′	Fermi	Long	L1V1	33	59
190830264	06:20:46	10 ^h 36 ^m 48 ^s	−54° 43′	Fermi	Ambiguous	H1V1 (HIL1V1)	242	331	478	31	45
190831332	07:57:31	4 ^h 22 ^m 31 ^s	14° 53′	Fermi	Long	L1V1	22	40
190831693	16:38:37	11 ^h 19 ^m 31 ^s	−22° 21′	Fermi	Long	HIL1V1	28	86
190901890	21:21:49	14 ^h 41 ^m 12 ^s	0° 56′	Fermi	Long	L1V1 [†]	22	29
190903722	17:19:36	04 ^h 09 ^m 43 ^s	−64° 8′	Fermi	Short	V1	66	87	133
190904174	04:11:00	2 ^h 23 ^m 40 ^s	−25° 02′	Fermi	Ambiguous	L1V1(H1V1)	84	109	154	7	12
190905985	23:38:28	15 ^h 37 ^m 55 ^s	3° 7′	Fermi	Short	V1	42	54	77
190906767	18:25:09	11 ^h 27 ^m 21 ^s	−71° 34′	Fermi	Long	HIL1V1	36	111
190910028	00:39:37	15 ^h 18 ^m 00 ^s	9° 04′	Fermi	Long	H1V1	33	54
190913155	03:43:09	16 ^h 53 ^m 21 ^s	44° 58′	Fermi	Short	H1V1 (HIL1V1)	201	250	382	9	15
190914345	08:16:34	1 ^h 13 ^m 45 ^s	21° 27′	Fermi	Long	L1V1 [†]	23	36
190915240	05:44:57	3 ^h 13 ^m 19 ^s	3° 59′	Fermi	Long	L1V1	25	42
190916590	14:10:14	21 ^h 25 ^m 04 ^s	−48° 54′	Fermi	Long	HIL1V1	23	170
190919764	18:20:02	23 ^h 49 ^m 26 ^s	−21° 49′	Fermi	Long	HIL1V1	73	234
190921699	16:45:55	22 ^h 33 ^m 31 ^s	−63° 25′	Fermi	Long	H1V1	32	46
190923617	14:48:02	0 ^h 32 ^m 48 ^s	−11° 01′	Fermi	Ambiguous	HIL1	133	162	239	32	80
190926A	09:52:16	6 ^h 42 ^m 27 ^s	59° 32′	Swift	Long	HIL1 [†]	72	186
190930400	09:36:06	15 ^h 52 ^m 52 ^s	−6° 05′	Fermi	Long	L1V1 [†]	22	30
191001279	06:41:50	20 ^h 20 ^m 47 ^s	15° 05′	Fermi	Long	H1V1	12	41

Note. The Satellite column lists the instrument the sky localization of which was used for GW analysis purposes. The Network column lists the GW detector network used in the analysis of each GRB: H1 = LIGO Hanford, L1 = LIGO Livingston, V1 = Virgo. A[†] denotes cases in which $T_{90} > 60$ s, so the on-source window of the generic transient search was extended to cover the GRB duration. For cases in which the generic transient search (Section 3.2) and the neutron star binary search (Section 3.1) used a different network, we report the network used by the latter in parentheses. Columns 8–12 display the 90% confidence exclusion distances to the GRB (D_{90}) for several emission scenarios: BNS, generic and aligned-spin NSBH, ADI-A, and CSG GW burst at 150 Hz with total radiated energy $E_{\text{GW}} = 10^{-2} M_{\odot} c^2$. The first three are determined with the neutron star binary search, while the last two are calculated with the generic transient search.

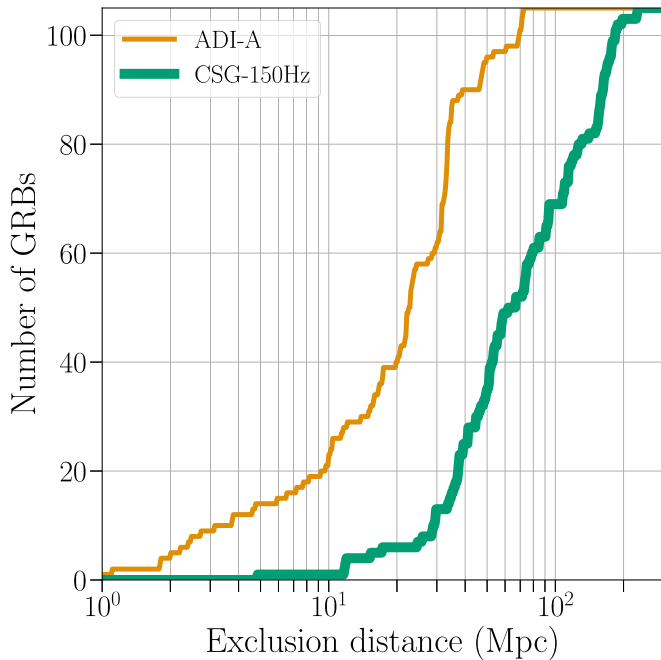


Figure 4. Cumulative histograms of the 90% confidence exclusion distances, D_{90} , for accretion disk instability (ADI; van Putten 2001; van Putten et al. 2014) signal model A (orange, thin line) and circular sine-Gaussian (CSG) 150 Hz (Abbott et al. 2017c) model (green, thick line). For a given GRB and signal model this is the distance within which 90% of simulated signals inserted into off-source data are successfully recovered with a significance greater than the loudest on-source trigger. The median values for ADI-A and CSG-150 waveforms are 23 Mpc and 73 Mpc, respectively.

method search (see Section 3.2), we provide population median exclusion limits, D_{90} , in Table 1. These vary roughly over one order of magnitude, which reflects the wide range of models used in the analysis. We report the D_{90} values found for each GRB in the case of ADI model A simulated signals and CSG simulated signals with central frequency of 150 Hz in Table 2.

4.1. GRB 190610A

For each event in the O3a sample that was localized with an error radius smaller than 0.5° , we searched GLADE (Dálya et al. 2018) for galaxies within 200 Mpc. We then compared the angular separation between each GRB and galaxy, and recorded all separations less than or equal to twice the error radius for each GRB. Of the 141 events in our sample, four had nearby galaxies according to the definition above: GRB 190530430, GRB 190531840, GRB 190610A, and GRB 190731943. Data for our GW follow-up analysis were available only in the case of the short GRB 190610A, first observed by Swift/BAT (Evans et al. 2019) and localized to within a 90% error radius of $1.9'$ (Lien et al. 2016; Palmer et al. 2019). On the edge of its localization region, there is a nearby galaxy at a luminosity distance of approximately 165 Mpc ($z = 0.037$), as reported in GLADE (see Figure 5).²¹² The angular separation between the center of the localization region and the nearby galaxy is at the 2.21σ level relative to the formal fit error, which is slightly less conservative than the quoted 90% localization derived from the S/N, and is

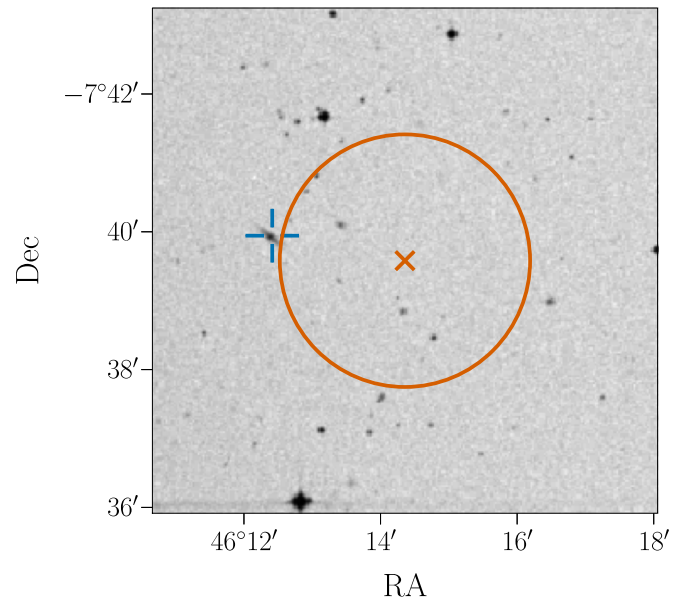


Figure 5. Overlay of the estimated 90% Swift/BAT error radius for GRB 190610A (orange circle) on the sky. A galaxy at around 165 Mpc (Dálya et al. 2018) compatible with this localization is indicated by the blue crosshair.

consistent with expectations of angular offsets from a host galaxy at that distance (Fong & Berger 2013).

We did not find any GW signal associated with GRB 190610A in the data available from the two LIGO detectors (Virgo data were not in observing mode at that particular time). Our modeled search described in Section 3.1, which uses an on-source window from -5 s to $+1$ s around the GRB trigger time, placed 90% confidence exclusion distances of 63 Mpc, 82 Mpc, and 114 Mpc for BNS binaries with generically oriented spins, NSBH binaries with generically oriented spins, and aligned-spin NSBH binaries (see Section 3.1 for more details on these three populations). In general, a distance of 165 Mpc can be within the reach of our modeled search, but GRB 190610A was in a sky location such that the sensitivity of both detectors was less than 30% of what it would have been in an optimal sky location.

5. Conclusions

We carried out targeted analyses for GWs associated with Fermi and Swift GRBs reported during the O3a LIGO–Virgo observing run. In the case of short and ambiguous GRBs events (see Section 2), we ran a modeled search for NS binary merger signals (Harry & Fairhurst 2011; Williamson et al. 2014), while an unmodeled search for GW transient signals was performed for all GRBs (Sutton et al. 2010; Was et al. 2012). As a result of our analyses, we found no GW signal in association with the GRBs that we followed up. This is consistent with the previously predicted rate of coincident detections of 0.1–1.4 per year for the third observing run of Advanced LIGO and Advanced Virgo (Abbott et al. 2017a). Additionally, by carrying out a weighted binomial test, we found no strong evidence for a population of unidentified subthreshold GW signals in our results. We set lower bounds on the distances to the progenitors of all GRBs we analyzed for a number of emission models. These D_{90} values are reported in Table 2, along with other information about each GRB that we considered; this includes timing, sky location, observing instrument, and GW detectors with available data. The

²¹² This galaxy can be found in the HyperLeda database (<http://leda.univ-lyon1.fr/>) under the identifier PGC 1015066 (Makarov et al. 2014), as well as the Sloan Digital Sky Survey under the identifier J030449.65-073956.6 (Alam et al. 2015).

90% confidence level exclusion distances achieved in this run include the largest values published so far for some individual GRBs (see Abbott et al. 2017c, 2019b). Among the GRBs we analyzed is GRB 190610A, the sky localization of which included a nearby galaxy at a luminosity distance of 165 Mpc. We placed 90% confidence level exclusion distances lower than this value for NS binary merger GW signals and are therefore unable to rule out the possibility that GRB 190610A occurred in such galaxy.

The authors gratefully acknowledge the support of the United States National Science Foundation (NSF) for the construction and operation of the LIGO Laboratory and Advanced LIGO as well as the Science and Technology Facilities Council (STFC) of the United Kingdom, the Max Planck Society (MPS), and the State of Niedersachsen/Germany for support of the construction of Advanced LIGO and construction and operation of the GEO600 detector. Additional support for Advanced LIGO was provided by the Australian Research Council. The authors gratefully acknowledge the Italian Istituto Nazionale di Fisica Nucleare (INFN), the French Centre National de la Recherche Scientifique (CNRS) and the Netherlands Organization for Scientific Research, for the construction and operation of the Virgo detector and the creation and support of the EGO consortium. The authors also gratefully acknowledge research support from these agencies as well as by the Council of Scientific and Industrial Research of India, the Department of Science and Technology, India, the Science & Engineering Research Board (SERB), India, the Ministry of Human Resource Development, India, the Spanish Agencia Estatal de Investigación, the Vicepresidència i Conselleria d'Innovació Recerca i Turisme and the Conselleria d'Educació i Universitat del Govern de les Illes Balears, the Conselleria d'Innovació Universitats, Ciència i Societat Digital de la Generalitat Valenciana and the CERCA Programme Generalitat de Catalunya, Spain, the National Science Centre of Poland and the Foundation for Polish Science (FNP), the Swiss National Science Foundation (SNSF), the Russian Foundation for Basic Research, the Russian Science Foundation, the European Commission, the European Regional Development Funds (ERDF), the Royal Society, the Scottish Funding Council, the Scottish Universities Physics Alliance, the Hungarian Scientific Research Fund (OTKA), the French Lyon Institute of Origins (LIO), the Belgian Fonds de la Recherche Scientifique (FRS-FNRS), Actions de Recherche Concertées (ARC) and Fonds Wetenschappelijk Onderzoek–Vlaanderen (FWO), Belgium, the Paris Île-de-France Region, the National Research, Development and Innovation Office Hungary (NKFIH), the National Research Foundation of Korea, the Natural Science and Engineering Research Council Canada, Canadian Foundation for Innovation (CFI), the Brazilian Ministry of Science, Technology, Innovations, and Communications, the International Center for Theoretical Physics South American Institute for Fundamental Research (ICTP-SAIFR), the Research Grants Council of Hong Kong, the National Natural Science Foundation of China (NSFC), the Leverhulme Trust, the Research Corporation, the Ministry of Science and Technology (MOST), Taiwan and the Kavli Foundation. The authors gratefully acknowledge the support of the NSF, STFC, INFN and CNRS for provision of computational resources.

We would like to thank all of the essential workers who put their health at risk during the COVID-19 pandemic, without whom we would not have been able to complete this work.

We would also like to thank Christian Malacaria and Aaron Tohuvavohu for providing useful comments that helped improve this paper.

Facilities: LIGO, EGO:Virgo, Fermi(GBM), Swift(BAT).

Software: LALSuite software library (LIGO Scientific Collaboration 2018), Matplotlib (Hunter 2007; Caswell et al. 2018), PyCBC (Nitz et al. 2020), X-Pipeline (Sutton et al. 2010; Was et al. 2012).

References

- Abadie, J., Abbott, B. P., Abbott, R., et al. 2012, *ApJ*, **760**, 12
- Abbott, B. P., Abbott, R., Abbott, T. D., et al. 2017a, *ApJL*, **848**, L13
- Abbott, B. P., Abbott, R., Abbott, T. D., et al. 2017b, *PhRvL*, **119**, 161101
- Abbott, B. P., Abbott, R., Abbott, T. D., et al. 2017c, *ApJ*, **841**, 89
- Abbott, B. P., Abbott, R., Abbott, T. D., et al. 2019a, *PhRvD*, **100**, 024017
- Abbott, B. P., Abbott, R., Abbott, T. D., et al. 2019b, *ApJ*, **886**, 75
- Abbott, B. P., Abbott, R., Abbott, T. D., et al. 2019c, *PhRvX*, **9**, 031040
- Abbott, B. P., Abbott, R., Abbott, T. D., et al. 2019d, *PhRvX*, **9**, 011001
- Abbott, B. P., Abbott, R., Abbott, T. D., et al. 2020a, *ApJL*, **892**, L3
- Abbott, B. P., Abbott, R., Abbott, T. D., et al. 2020b, *ApJL*, **896**, L44
- Abbott, B. P., Abbott, R., Abbott, T. D., et al. 2020c, *PhRvD*, **101**, 084002
- Abbott, R., Abbott, T. D., Abraham, S., et al. 2021, *PhRvX*, **11**, 021053
- Alam, S., Albareti, F. D., Allende Prieto, C., et al. 2015, *ApJS*, **219**, 12
- Allen, B., Anderson, W. G., Brady, P. R., Brown, D. A., & Creighton, J. D. 2012, *PhRvD*, **85**, 122006
- Aloy, M. A., Janka, H.-T., & Müller, E. 2005, *A&A*, **436**, 273
- Aloy, M. A., Mueller, E., Ibanez, J. M., Marti, J. M., & MacFadyen, A. 2000, *ApJL*, **531**, L119
- Arun, K. G., Buonanno, A., Faye, G., & Ochsner, E. 2009, *PhRvD*, **79**, 104023 [Erratum: *PhRvD* 84, 049901(2011)]
- Babak, S., Taracchini, A., & Buonanno, A. 2017, *PhRvD*, **95**, 024010
- Barthelmy, S. D., Barbier, L. M., Cummings, J. R., et al. 2005, *SSRv*, **120**, 143
- Beniamini, P., Granot, J., & Gill, R. 2020, *MNRAS*, **493**, 3521
- Berger, E. 2011, *NewAR*, **55**, 1
- Berger, E. 2014, *ARA&A*, **52**, 43
- Berger, E., Fong, W., & Chornock, R. 2013, *ApJL*, **774**, L23
- Biscoveanu, S., Thrane, E., & Vitale, S. 2020, *ApJ*, **893**, 38
- Blanchet, L., Iyer, B. R., Will, C. M., & Wiseman, A. G. 1996, *CQGrA*, **13**, 575
- Blinnikov, S. I., Novikov, I. D., Perevodchikova, T. V., & Polnarev, A. G. 1984, *SvAL*, **10**, 177
- Bloom, J. S., Prochaska, J. X., Pooley, D., et al. 2006, *ApJ*, **638**, 354
- Bohé, A., Faye, G., Marsat, S., & Porter, E. K. 2015, *CQGrA*, **32**, 195010
- Bohé, A., Marsat, S., & Blanchet, L. 2013, *CQGrA*, **30**, 135009
- Burlon, D., Ghirlanda, G., Ghisellini, G., et al. 2008, *ApJL*, **685**, L19
- Burlon, D., Ghirlanda, G., Ghisellini, G., Greiner, J., & Celotti, A. 2009, *A&A*, **505**, 569
- Burns, E., Tohuvavohu, A., Buckley, J., et al. 2019, *BAAS*, **51**, 38
- Capano, C., Harry, I., Privitera, S., & Buonanno, A. 2016, *PhRvD*, **93**, 124007
- Castro-Tirado, A., de Ugarte Postigo, A., Gorosabel, J., et al. 2005, *A&A*, **439**, L15
- Caswell, T. A., Droettboom, M., Hunter, J., et al. 2018, matplotlib/matplotlib v2.2.3, Zenodo, doi:10.5281/zenodo.1343133
- Chen, H.-Y., Holz, D. E., Miller, J., et al. 2021, *CQGrA*, **38**, 055010
- Ciolfi, R., Kastaun, W., Kalinani, J. V., & Giacomazzo, B. 2019, *PhRvD*, **100**, 023005
- Corsi, A., & Meszaros, P. 2009, *ApJ*, **702**, 1171
- Coughlin, M. W., Dietrich, T., Antier, S., et al. 2020, *MNRAS*, **492**, 863
- Coyne, R. 2015, PhD thesis, The George Washington Univ.
- Dai, Z. G., & Gou, L. J. 2001, *ApJ*, **552**, 72
- Dal Canton, T., & Harry, I. W. 2017, arXiv:1705.01845
- Dálya, G., Galgóczi, G., Dobos, L., et al. 2018, *MNRAS*, **479**, 2374
- Davies, M. B., King, A., Rosswog, S., & Wynn, G. 2002, *ApJL*, **579**, L63
- Eichler, D., Livio, M., Piran, T., & Schramm, D. N. 1989, *Natur*, **340**, 126
- Evans, P. A., Gropp, J., Kennea, J. A., et al. 2019, *GCN Circ.*, 24775, <https://gcn.gsfc.nasa.gov/gcn3/24775.gcn3>
- Farah, A., Essick, R., Doctor, Z., Fishbach, M., & Holz, D. E. 2020, *ApJ*, **895**, 108
- Finn, L. S., & Chernoff, D. F. 1993, *PhRvD*, **47**, 2198
- Fong, W., & Berger, E. 2013, *ApJ*, **776**, 18
- Fong, W., Blanchard, P. K., Alexander, K. D., et al. 2019, *ApJL*, **883**, L1
- Fong, W.-f., Berger, E., Margutti, R., & Zauderer, B. A. 2015, *ApJ*, **815**, 102
- Foucart, F., Hinderer, T., & Nissanke, S. 2018, *PhRvD*, **98**, 081501
- Fryer, C. L., Holz, D. E., & Hughes, S. A. 2002, *ApJ*, **565**, 430

- Fryer, C. L., & New, K. C. B. 2011, *LRR*, **14**, 1
- Galama, T. J., Vreeswijk, P. M., van Paradijs, J., et al. 1998, *Natur*, **395**, 670
- Gehrels, N., Barbier, L., Barthelmy, S. D., et al. 2005, *Natur*, **437**, 851
- Gehrels, N., Chincarini, G., Giommi, P., et al. 2004, *ApJ*, **611**, 1005
- Ghirlanda, G., Salafia, O. S., Paragi, Z., et al. 2019, *Sci*, **363**, 968
- Gill, R., & Granot, J. 2018, *MNRAS*, **478**, 4128
- Goldstein, A., Veres, P., Burns, E., et al. 2017, *ApJL*, **848**, L14
- Gossan, S. E., Sutton, P. J., Stuver, A., et al. 2016, *PhRvD*, **93**, 042002
- Gottlieb, O., Nakar, E., & Piran, T. 2018a, *MNRAS*, **473**, 576
- Gottlieb, O., Nakar, E., Piran, T., & Hotokezaka, K. 2018b, *MNRAS*, **479**, 588
- Gruber, D., Goldstein, A., Weller von Ahlefeld, V., et al. 2014, *ApJS*, **211**, 12
- Hallinan, G., Corsi, A., Mooley, K. P., et al. 2017, *Sci*, **358**, 1579
- Hamburg, R., Fletcher, C., Burns, E., et al. 2020, *ApJ*, **893**, 100
- Harry, I. W., & Fairhurst, S. 2011, *PhRvD*, **83**, 084002
- Hayes, F., Heng, I. S., Veitch, J., & Williams, D. 2020, *ApJ*, **891**, 124
- Hessels, J. W. T., Ransom, S. M., Stairs, I. H., et al. 2006, *Sci*, **311**, 1901
- Hjorth, J., & Bloom, J. S. 2012, in *The Gamma-Ray Burst—Supernova Connection*, ed. C. Kouveliotou, R. A. M. J. Wijers, & S. Woosley (Cambridge: Cambridge Univ. Press), 169
- Hjorth, J., Sollerman, J., Møller, P., et al. 2003, *Natur*, **423**, 847
- Hoseinzadeh, G., Cowperthwaite, P. S., Gomez, S., et al. 2019, *ApJL*, **880**, L4
- Hunter, J. D. 2007, *CSE*, **9**, 90
- Husa, S., Khan, S., Hannam, M., et al. 2016, *PhRvD*, **93**, 044006
- Japelj, J., Kann, D. A., de Ugarte Postigo, A., et al. 2019, *GCN Circ.*, 24916, <https://gcn.gsfc.nasa.gov/gcn3/24916.gcn3>
- Kasliwal, M. M., Nakar, E., Singer, L. P., et al. 2017, *Sci*, **358**, 1559
- Khan, S., Husa, S., Hannam, M., et al. 2016, *PhRvD*, **93**, 044007
- Kiziltan, B., Kottas, A., De Yoreo, M., & Thorsett, S. E. 2013, *ApJ*, **778**, 66
- Kobayashi, S., & Meszaros, P. 2003, *ApJ*, **589**, 861
- Koshut, T. M., Kouveliotou, C., Paciasas, W. S., et al. 1995, *ApJ*, **452**, 145
- Kouveliotou, C., Meegan, C. A., Fishman, G. J., et al. 1993, *ApJL*, **413**, L101
- Kreidberg, L., Bailyn, C. D., Farr, W. M., & Kalogera, V. 2012, *ApJ*, **757**, 36
- Kumar, P., & Zhang, B. 2014, *PhR*, **561**, 1
- Lamb, G. P., & Kobayashi, S. 2017, *MNRAS*, **472**, 4953
- Lazzati, D. 2005, *MNRAS*, **357**, 722
- Lazzati, D., Deich, A., Morsony, B. J., & Workman, J. C. 2017, *MNRAS*, **471**, 1652
- Lazzati, D., Morsony, B. J., & Begelman, M. 2009, *ApJL*, **700**, L47
- Lazzati, D., Perna, R., Morsony, B. J., et al. 2018, *PhRvL*, **120**, 241103
- Lee, W. H., & Ramirez-Ruiz, E. 2007, *NJPh*, **9**, 17
- Lien, A., Sakamoto, T., Barthelmy, S. D., et al. 2016, *ApJ*, **829**, 7
- LIGO Scientific Collaboration 2018, LIGO Algorithm Library, doi:10.7935/GT1W-FZ16
- Lipunov, V. M., Postnov, K. A., & Prokhorov, M. E. 2001, *ARep*, **45**, 236
- Liu, T., Hou, S.-J., Xue, L., & Gu, W.-M. 2015, *ApJS*, **218**, 12
- Lundquist, M. J., Paterson, K., Fong, W., et al. 2019, *ApJL*, **881**, L26
- MacFadyen, A. I., Woosley, S. E., & Heger, A. 2001, *ApJ*, **550**, 410
- Makarov, D., Prugniel, P., Terekhova, N., Courtois, H., & Vauglin, I. 2014, *A&A*, **570**, A13
- Makhathini, S., Mooley, K. P., Brightman, M., et al. 2020, arXiv:2006.02382
- Martin-Carrillo, A., Savchenko, V., Ferrigno, C., et al. 2019, *GCN Circ.*, 24169, <https://gcn.gsfc.nasa.gov/gcn3/24169.gcn3>
- Mazets, E. P., Golenetskii, S. V., Il'inskiĭ, V. N., et al. 1981, *Ap&SS*, **80**, 3
- Meegan, C., Lichti, G., Bhat, P. N., et al. 2009, *ApJ*, **702**, 791
- Mikoczi, B., Vasuth, M., & Gergely, L. A. 2005, *PhRvD*, **71**, 124043
- Miller, M. C., & Miller, J. M. 2014, *PhR*, **548**, 1
- Mishra, C. K., Kela, A., Arun, K. G., & Faye, G. 2016, *PhRvD*, **93**, 084054
- Mogushi, K., Cavaglià, M., & Siellez, K. 2019, *ApJ*, **880**, 55
- Mooley, K. P., Deller, A. T., Gottlieb, O., et al. 2018, *Natur*, **561**, 355
- Murguia-Berthier, A., Ramirez-Ruiz, E., Montes, G., et al. 2017, *ApJL*, **835**, L34
- Nakar, E. 2007, *PhR*, **442**, 166
- Narayan, R., Paczynski, B., & Piran, T. 1992, *ApJL*, **395**, L83
- Narayana Bhat, P., Meegan, C. A., von Kienlin, A., et al. 2016, *ApJS*, **223**, 28
- Nitz, A., Harry, I., Brown, D., et al. 2020, gwastro/pycbc: PyCBC, v1.16.6, Zenodo, doi:10.5281/zenodo.3961510
- Norris, J. P., Cline, T. L., Desai, U. D., & Teegarden, B. J. 1984, *Natur*, **308**, 434
- Ott, C. D., & Santamaría, L. 2013, *Gravitational Wave Emission from Accretion Disk Instabilities—Analytic Models*, Tech. Rep., LIGO-T1100093
- Owen, B. J., & Sathyaprakash, B. S. 1999, *PhRvD*, **60**, 022002
- Özel, F., Psaltis, D., Narayan, R., & McClintock, J. E. 2010, *ApJ*, **725**, 1918
- Paczynski, B. 1986, *ApJL*, **308**, L43
- Paczynski, B. 1991, *AcA*, **41**, 257
- Palmer, D. M., Darthelmy, S. D., Cummings, J. R., et al. 2019, *GCN Circ.*, 24783, <https://gcn.gsfc.nasa.gov/gcn3/24783.gcn3>
- Pan, Y., Buonanno, A., Taracchini, A., et al. 2014, *PhRvD*, **89**, 084006
- Pannarale, F., & Ohme, F. 2014, *ApJL*, **791**, L7
- Piro, A. L., & Pfahl, E. 2007, *ApJ*, **658**, 1173
- Popham, R., Woosley, S., & Fryer, C. 1999, *ApJ*, **518**, 356
- Pozanenko, A., Minaev, P., Grebenev, S., & Chelovekov, I. 2020, *Astron. Lett.*, **45**, 710
- Radice, D., Morozova, V., Burrows, A., Vartanyan, D., & Nagakura, H. 2019, *ApJL*, **876**, L9
- Romero, G. E., Reynoso, M. M., & Christiansen, H. R. 2010, *A&A*, **524**, A4
- Rossi, A., Heintz, K. E., Fynbo, J. P. U., et al. 2019, *GCN Circ.*, 25252, <https://gcn.gsfc.nasa.gov/gcn3/25252.gcn3>
- Rossi, E., Lazzati, D., & Rees, M. J. 2002, *MNRAS*, **332**, 945
- Sathyaprakash, B. S., & Dhurandhar, S. V. 1991, *PhRvD*, **44**, 3819
- Savchenko, V., Ferrigno, C., Kuulkers, E., et al. 2017, *ApJL*, **848**, L15
- Shibata, M., Karino, S., & Eriguchi, Y. 2003, *MNRAS*, **343**, 619
- Stanek, K. Z., Matheson, T., Garnavich, P. M., et al. 2003, *ApJL*, **591**, L17
- Sutton, P. J., Jones, G., Chatterji, S., et al. 2010, *NJPh*, **12**, 053034
- Svinkin, D., Golenetskii, S., Aptekar, R., et al. 2019, *GCN Circ.*, 24417, <https://gcn.gsfc.nasa.gov/gcn3/24417.gcn3>
- Tanvir, N. R., Levan, A. J., Fruchter, A. S., et al. 2013, *Natur*, **500**, 547
- Taracchini, A., Buonanno, A., Pan, Y., et al. 2014, *PhRvD*, **89**, 061502
- Tohuvavohu, A., Kennea, J. A., DeLaunay, J., et al. 2020, *ApJ*, **900**, 35
- Troja, E., Piro, L., van Eerten, H., et al. 2017, *Natur*, **551**, 71
- Troja, E., van Eerten, H., Zhang, B., et al. 2020, *MNRAS*, **498**, 5643
- Usov, V. V. 1992, *Natur*, **357**, 472
- Valeev, A. F., Castro-Tirado, A. J., Hu, Y.-D., et al. 2019, *GCN Circ.*, 25565, <https://gcn.gsfc.nasa.gov/gcn3/25565.gcn3>
- van Putten, M. H. P. M. 2001, *PhRvL*, **87**, 091101
- van Putten, M. H. P. M., Lee, G. M., Della Valle, M., Amati, L., & Levinson, A. 2014, *MNRAS*, **444**, L58
- Vedrenne, G., & Atteia, J.-L. 2009, *Gamma-Ray Bursts: The Brightest Explosions in the Universe* (Berlin: Springer)
- Veres, P., Mészáros, P., Goldstein, A., et al. 2018, arXiv:1802.07328
- von Kienlin, A., Meegan, C. A., Paciasas, W. S., et al. 2014, *ApJS*, **211**, 13
- Wang, X.-Y., & Meszaros, P. 2007, *ApJ*, **670**, 1247
- Was, M., Sutton, P. J., Jones, G., & Leonor, I. 2012, *PhRvD*, **86**, 022003
- Williams, D., Clark, J. A., Williamson, A. R., & Heng, I. S. 2018, *ApJ*, **858**, 79
- Williamson, A. R., Biwer, C., Fairhurst, S., et al. 2014, *PhRvD*, **90**, 122004
- Woosley, S. E. 1993, *ApJ*, **405**, 273
- Wu, Y., & MacFadyen, A. 2018, *ApJ*, **869**, 55
- Zhang, B. 2019, *FrPhy*, **14**, 64402
- Zhang, B., & Meszaros, P. 2001, *ApJL*, **552**, L35
- Zhang, B., & Mészáros, P. 2002, *ApJ*, **571**, 876
- Zhang, B. B., Zhang, B., Sun, H., et al. 2018, *NatCo*, **9**, 447
- Zhang, W., Woosley, S. E., & MacFadyen, A. I. 2003, *ApJ*, **586**, 356